August 2019

Optimizing Self-Healing Wind Turbine Blades Utilizing Dicyclopentadiene Infused Vascular Networks

GIOVANNI LEWINSKI
University of Wisconsin-Milwaukee

OPTIMIZING SELF-HEALING WIND TURBINE BLADES UTILIZING DICYCLOPENTADIENE INFUSED VASCULAR NETWORKS

by

Giovanni Al-Muhairi Lewinski

A Thesis Submitted in

Partial Fulfillment of the

Requirements for the Degree of

Master of Science

in Engineering

at

The University of Wisconsin- Milwaukee

August 2019

ABSTRACT

OPTIMIZING SELF-HEALING WIND TURBINE BLADES
BY UTILIZING DICYCLOPENTADIENE INFUSED VASCULAR NETWORKS
by

Giovanni Al-Muhairi Lewinski

The University of Wisconsin-Milwaukee, 2019
Under the Supervision of Professor Ryoichi S. Amano

Self-healing wind turbine blades can reduce costs associated with maintenance, repair, and energy compensation. Self-healing is the ability to sustain and recover from damage autonomously. The self-healing presented in this paper uses the reaction of two agents Dicyclopentadiene, DCPD, and Grubbs' first-generation catalyst, henceforward known as a catalyst to fuel this recovery. DCPD is housed as a liquid isolated from the catalyst until a damaging event occurs, causing the two agents to mix and solidify to form the thermoset Polydicyclopentadiene, PDCPD. We discuss the efforts made to optimize the self-healing properties of wind turbine blades and provide new systems to maximize this offset. The first method involves copper wire coated by paraffin wax embedded into a fiber-reinforced polymer, FRP, samples incorporated with catalyst. The wires were extracted from cured samples to create cavities that were then injected with the healing agent, DCPD. To evaluate the healing system's effect in a real-life application, a prototype wind turbine was fabricated and wind tunnel testing was conducted. After 24 hours of curing time, Raman spectroscopy was performed to determine

the level of the DCPD's reaction with the catalyst to create PDCPD. The second method utilizes 3D printed templates to imprint a vascular network in a single glass fiber FRP sheet, which is infused with DCPD and later embedded into a multilayer FRP. The catalyst was incorporated into either the single layer or the multi-layer sample to promote self-healing. Using ultraviolet lighting to highlight DCPD mixed with UV fluorescent dye movement during Three-point bending flexural testing, the storage, and transport processes of the healing agent were observed. The flexural tests were performed to obtain the maximum flexural strengths of the FRP samples before and after recovery. By comparing the flexural test results before and after healing for each method, a hierarchy was created in terms of percent recovery.

TABLE OF CONTENTS

LIST OF FIGURES

LIST OF TABLES

LIST OF ABBREVIATIONS

ABS	Acrylonitrile Butadiene Styrene
DCPD	Dicyclopentadiene
FRP	Fiber Reinforced Polymer
PDCPD	Polydicyclopentadiene
PLA	Polylactic Acid
ROMP	Ring-opening Metathesis Polymerization
UV	Ultraviolet
VARTM	Vacuum Assisted Resin Transfer Molding

ACKNOWLEDGMENTS

I would first like to thank my thesis advisor Professor Amano at the University of Wisconsin-Milwaukee for being a continuous source of support.

I would also like to thank Rulin Shen for co-authoring “A New Vascular System Highly Efficient in the Storage and Transport of Healing Agent for Self-Healing Wind Turbine Blades” as well as his tremendous effort put into the research of self-healing vascular networks.

I would also like to acknowledge Arun Matt for providing a solid foundation for this research.

NSF funded the research under CBET No. 1236312.

Parts of “ A New Vascular System Highly Efficient in the Storage and Transport of Healing Agent for Self-Healing Wind Turbine Blades” have been previously published as [1]

CHAPTER 1: INTRODUCTION

Self-healing wind turbine blades could reduce costs associated with maintenance, repair, and energy compensation. With ongoing efforts to reduce reliance on fossil fuels, the U.S Department of Energy has targeted 20% of all U.S electricity to stem from renewable sources by 2030, and 20% of that energy is expected to come from wind energy [2]. To maximize the energy output of wind turbines, great strides have been taken using composites to increase the overall size of wind turbines [3]. Composite materials are excellent candidates because of their high strength to weight ratio, but scaling has it limits [4]. Furthermore, onshore wind turbine installations on complex terrain are increasing [5]. Self-healing blades would be able to help combat these obstacles by increasing the overall durability of wind turbine blades by healing cracks before they can propagate making larger blades and inaccessible blades more feasible. More durable blades could, in turn, reduce costs for energy compensations from energy sources such as coal plants which can take upwards of seven hours to start [6].

In this study, paraffin wax coated copper wires were embedded and extracted from FRP samples to produce various vascular networks to encase the healing agent rather than incorporating separate healing agent filled vessels as used in previous studies. To evaluate the amount of recovery and effects on sample strength for each of the healing networks, both self-healing FRP sheets and wind turbine blades were created. Three-point bending flexural testing was used to assess the healing ability of the self-healing sheets through the comparison of maximum flexural stresses before and after healing. Flexural testing is the ideal tool to evaluate sample recovery because of its similarity to the loading enacted on actual wind turbine blades. [7]. Furthermore, through the addition of UV light reactive dye to the healing agent, flexural testing highlights the

healing agent storage and transport processes. Raman spectroscopy, as a non-destructive test method, was also used to determine the extent of the healing agent polymerized in the self-healing blade.

The second method examined involves the use of vascular network imprinted FRP. 3D printed ABS hexagonal, and square grids were mounted to glass and used as the bottom surface for the VARTM apparatus used in creating test samples. Resulting single layer samples, imprint samples, were infused with DCPD. These imprint samples were embedded as a layer in a larger six-layer sample. First-generation Grubbs' catalyst was dispersed in either the imprint layer itself or the epoxy of the larger sample to create samples capable of self-healing. Hexagonal and grid configurations were chosen for three reasons. Using the other healing methods mentioned previously, such configurations would be impossible. Both patterns create one singular DCPD reservoir crossing the samples. Both the wire method and the method proposed in this paper have 100% storage efficiencies with storage efficiency determined as the ratio of the cross-sectional area occupied by the vessel to the cross-sectional area occupied by the healing agent. Like the wire removal method, flexural testing was used to evaluate sample strength and healing performance.

CHAPTER 2: LITERATURE REVIEW

The prevalent theme for self-healing polymer composite research is the creation and development of new methods to instill those self-healing capabilities. White et al. [8] devised the concept of using encapsulated DCPD in conjunction with Grubb's first-generation catalyst dispersed throughout an epoxy matrix to create a self-healing polymer, as shown in Figure 1.

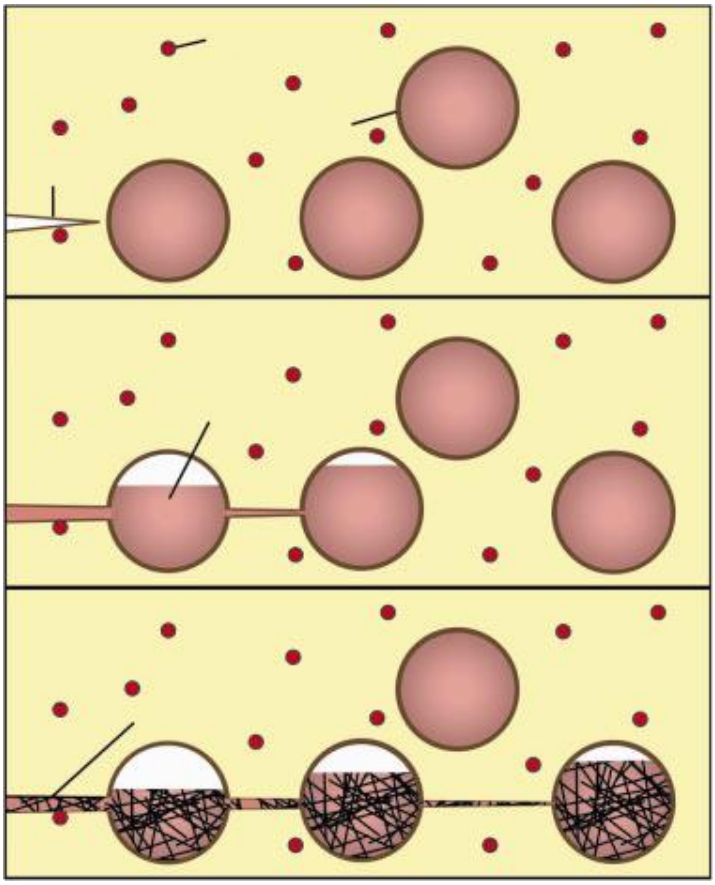

Figure 1: The autonomic healing concept. A microencapsulated healing agent is embedded in a structural composite matrix containing a catalyst capable of polymerizing the healing agent. (Top): Cracks form in the matrix wherever damage occurs; (Middle); the crack ruptures the microcapsules, releasing the healing agent into the crack plane through capillary action; (Bottom); the healing agent contacts the catalyst, triggering polymerization that bonds the crack faces closed [7].

The method relies on the brittle fracture of a modified epoxy matrix to rupture DCPD capsules and release the housed DCPD. The housed DCPD then flows into the crack where the ensuing reaction with surrounding catalyst would create the polymer PDCDP. To ensure proper dispersal of DCPD within the system, stiffness studies were performed, and the capsule wall was designed to rupture when encountering impending cracks rather than deflecting the cracks another location. The studies showed that the thicker capsules would deflect the crack away from the capsule while a thinner capsule would rupture as desired. To determine the efficiency of the capsule method, three avenues were approached, environmental scanning electron microscopy, infrared spectroscopy, and tapered double-cantilever beam samples. The first two non-destructive tests check for the presence of PDCDP on the fractured surface, and the amount of PDCDP absorbed into the sample, respectively. The third method applied to a load to the center of a notched sample twice before and after to determine recovery percentages. The results of the study showed a 75% recovery of initial strength. The flaw in this method is the sporadic dispersion of the healing capsules within the healing matrix. With this method, there is a chance that a crack could propagate and not rupture enough if any capsules to heal fully. The only way to ensure healing would be to increase the concentration of the healing capsules at the cost of sample strength.

Toohey et al. [9] introduced a method of creating healing vascular networks using direct-write assembly with fugitive organic ink with the intention of mimicking blood vessels. The process involved using a three-axis nozzle able to dispense and create a lattice structure of fugitive organic ink. Epoxy would flow around the organic ink, which would later be melted away

creating the vascular network. The network would then be injected with DCPD which would then react with Grubbs' catalyst dispersed throughout the epoxy. The process would allow samples to be fractured and healed approximately seven times. Recovery rates of approximately 60% were evaluated using four-point bending. Hansen et al. [10] later improved upon the process by using two types of fugitive organic ink. One ink composed of an aqueous, triblock-copolymer solution would soften at a temperature below 5°C and the second ink would liquefy at temperatures above 80°C. Removing the inks separately allows the levels of the lattice structure to be filled with alternating epoxy and epoxy hardener, as shown in Figure 2.

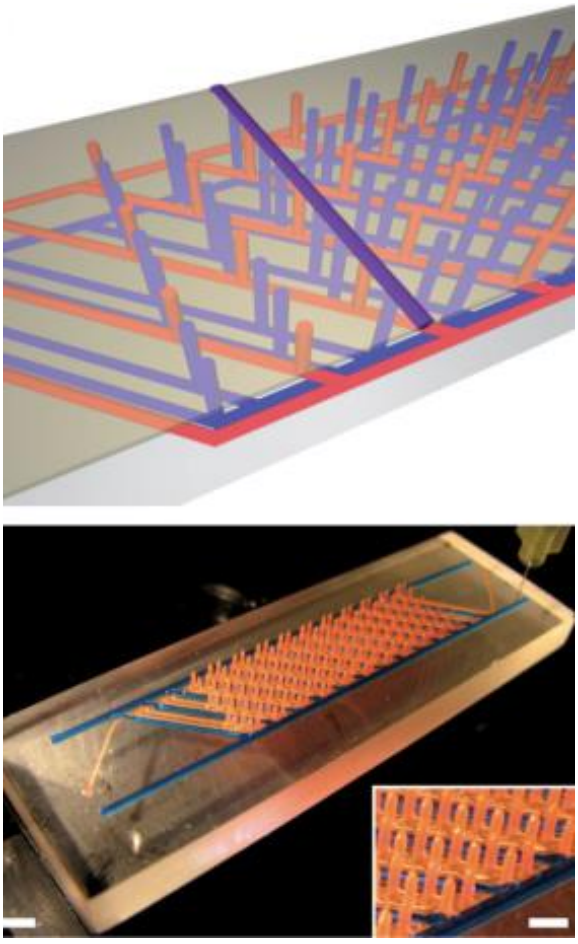

Figure 2: (Top) Schematic view of an interpenetrating microvascular network that supplies two fluids (red and blue) to a crack plane, where mixing occurs (purple). (Bottom) Interpenetrating microvascular network fabricated by the direct-write assembly of wax (orange)- and pluronic (blue)-based fugitive inks [10].

Recovery percentages reached near 100% in some instances, and healing was able to be repeated more than 30 times. The authors point out that one limitation to the method is the distance between the epoxy and hardener layers, increasing the needed crack depth to facilitate healing within the sample. Furthermore, the use of the direct-write assembly method limits the vascular network geometry to configurations made from one continuous line, and the sample size is restricted to the bed size of the machine used. Additionally, the form the samples correctly the epoxy used is limited to that of a low viscosity grade and is poured over the vascular network eliminating other composite creation methods such as VARTM and wet lay up as an option.

Like the direct-write assembly method, Partick et al. [11] created a vascular network without vessels housing epoxy and hardener separately until sample failure caused the two separate chemicals to react and heal the structure. PLA, polylactic acid, was woven through glass fiber sheets before using VARTM to create epoxy FRP samples, as shown in Figure 3.

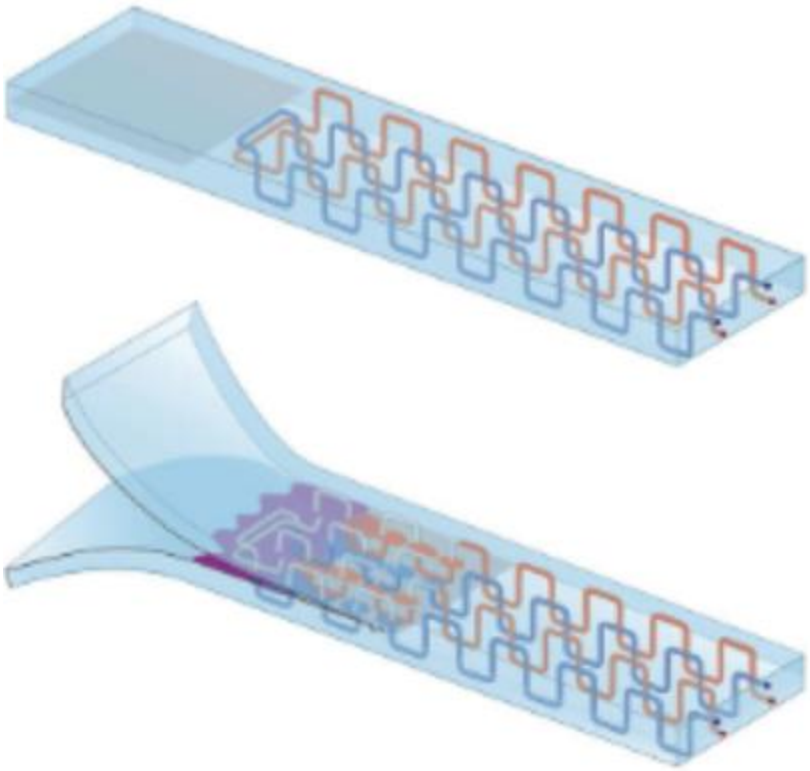

Figure 3: Schematic of microvascular double cantilever beam (DCB) fracture specimen with dual-channel (red/blue) vascular network where fracture triggers the release of liquid healing agents from ruptured microchannels [11].

Epoxy with a glass transition temperature of 150° C was used to create the samples. After fully cured the samples were heated to 200° C to liquefy the PLA and exposed to a vacuum to evacuate the PLA. The resulting cavities were injected with either epoxy or hardener to instill the self-healing capability. The negatives of this approach the need to heat the entire sample past the glass transition point and the need for the vacuum to remove the PLA. For larger samples, this would be unfeasible. Once past the glass transition point, any structure would lose its integrity and the amount of vacuum needed to purge a small diameter jogging vascular network would be substantial.

Motuku et al. [12] chose hollow glass fibers, 1.15 mm outside diameter borosilicate glass microcapillary pipettes, flint glass Pasteur pipettes, copper tubing, and aluminum tubing in plain weave fiberglass fabric reinforced polymer composites to study and determine the optimal material to supply DCPD to emerging crack zones in VARTM created glass-reinforced epoxy. Motuku et al. [12] concluded that the borosilicate glass microcapillary pipettes were the best material to provide the healing agent because of its comparable impact strength to that of the without-pipettes control composite. Matt et al. [13] continued the research in the pursuits of optimizing self-healing VARTM created FRP samples utilizing .5 mm outside diameter borosilicate tubes, as shown in Figure 4.

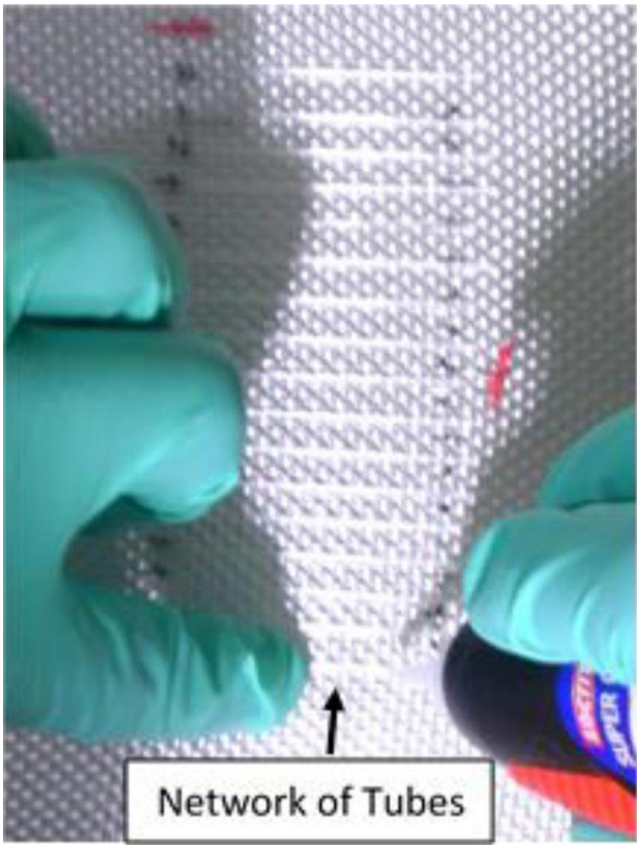

Figure 4: Photograph of the tubes being placed with small drops of glue to hold them in place over the glass fiber [14].

Various samples made from epoxy reinforced with 6 layers of glass fiber sheeting were created with DCPD borosilicate tubes placed between different layers of glass fiber to compose the central layer, penultimate layer, and final layer. Three-point bending tests were performed to determine which location of the tubes provided the highest performing sample in terms of flexural strength and percent recovery. The central layer placement of the tubes proved optimal offering an average recovery of 92.12% and 25% reduction in strength. The main obstacle from the borosilicate tube method to create self-healing samples stems from the delicateness of the glass combine with the installation of the tubes within the sample. To ensure proper healing, the glass tubes must be accurately places and adhered to a glass sheet before starting the VARTM process. Moreover, the vascular system created by the tubes is disjointed. The inclusion of individual tubes would limit the amount of DCPD available by constricting the movement of DCPD within the sample. Lastly, the glass itself weakens the sample by replacing the epoxy with a lower strength material. The goal of this paper is to improve on the limitations discussed for each method described.

CHAPTER 3: METHODS

3.1 Wire Formed Vascular Network Method

Per Matt et al. [13] DCPD was selected as the healing agent to work with Grubbs' first-generation catalyst to initiate polymerization. On the same basis, marine epoxy resin and fiberglass fabric (0.23 kg/m^2, 0.27 mm thick, and 16×14 plain weave) composite components were chosen as wind turbine blade representative materials. By industry standards, the VARTM process was employed to mold the FRP sample sheets. Six layers of fiberglass fabric with the fiberglass weaving running parallel and perpendicular to the VARTM flow was used in every sheet sample.

3.1.1 Wire Formed Vascular Network Sample Creation

Three materials were trialed in forming the vascular networks, paraffin wax coated cotton thread, .5 mm nickel-chromium wire and .5 mm copper wire. The materials were placed in the center layer before VARTM on 6 mm intervals. The materials were chosen because their size and circular profile were close to the borosilicate tubes used by Matt et al. [15]. Paraffin wax was selected as the coating because of its low melting temperature relative to epoxy and its uses as both a protective barrier and lubricant. Nickel-chromium wire and copper wire provided similar results. However, the copper wire was stiffer more natural to uncoil and straighten before configuring the vascular network. Additionally, the added strength prevented the copper wire from breaking during extraction.

After verifying that paraffin wax coated copper wires were the optimal method for treating vascular networks, self-healing samples of different network configurations were created. The first sample, the control sample, was produced without a vascular network. The second sample embedded a one-directional set of wires parallel to the VARTM flow placed in the center layer. The third sample embedded two one-directional sets of wires parallel to flow, with one set located above the second and the fourth layer, as shown in Figure 5.

Figure 5: Uncoiled and straightened wire arranged in a grid configuration in the center layer of the sample with the ends of the wire extended past the perimeter of the glass fiber sheets to aid in removal.

A fourth sample embedded a two-directional grid, one set of wires running parallel to the flow and another set placed on top of wires running perpendicular to the flow stream positioned within the center layer. Three total sample configurations were used for all three test samples, a single-center layer network, two penultimate layer networks, and a stacked grid network, as presented in Figure 6 and Table 1.

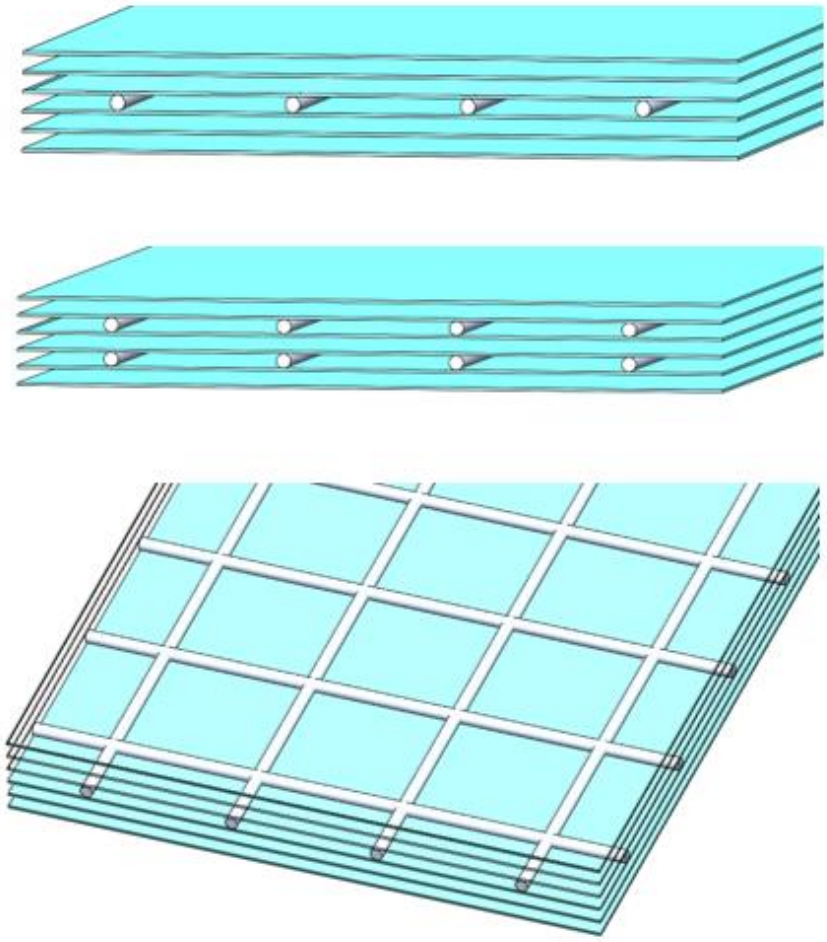

Figure 6: 3D model representations of copper wires placed between fiberglass sheets. Top, copper wires in center layer. Center, copper wires in penultimate layers. Bottom, overlapping copper wires forming a grid in center layer.

Table 1: Tabulated samples with substrate used to form networks, the use of a catalyst, and network layout.

Sample number	Embeded Material	Healing Agent and Catalyst Present?	Vascular Network Layout and Location
Sample 1	Control	No	N/A
Sample 2	Copper	Yes	1-Dir., center-layer
Sample 3	Copper	Yes	1-Dir., the second and the penultimate-layer
Sample 4	Copper	Yes	2-Dir., center-layer

3.1.2 Wire Formed Vascular Network Sample Test Preparation

Samples 1-4 were cut into 12.7 mm wide strips for flexural testing. Unlike in the previously mentioned studies, the healing agent could only be added to the cured samples. Before cutting the samples for testing, the samples were heated to 120 °C to melt the paraffin wax coating the wires to aid in the wire extraction and to remove any residual paraffin wax from the samples. Before injecting the samples with a healing agent, the DCPD was heated in an oven to 150 °C for approximately 2 minutes to liquefy the compound [15] completely. Each network cavity was injected with DCPD mixed with UV light reactive dye to highlight the DCPD's movement during flexural testing, as shown in Figure 7.

Figure 7: Wire formed network incorporated samples injected with DCPD.

The exposed openings of the networks were sealed using a standard adhesive. The prepared samples were subjected to three-point bending flexural tests, samples tested once, referred to as unhealed samples and samples tested twice, before and after healing, are referred to as healed samples. The untested bending test samples were heated for approximately 2 minutes in an oven at 150°C to ensure that the DCPD was entirely liquefied within the samples before flexural testing [15]. The unhealed samples after testing were placed flat below a dead weight for 24 hours. According to Kessler et al. [16], the healing time is dependent on local catalyst

concentration and that longer healing times (>1500 min) provided optimal results so, the unhealed samples were subjected to another round of bending tests after a healing time of 24 hours.

Three-point bending test samples were prepared and tested according to ASTM D7264 “Standard test method for flexural properties of polymer matrix composite materials” [17]. The cross-head rate was 1.27 mm/min, and a span to thickness ratio of 32:1 was maintained. The three-point bending tests were stopped immediately at the onset of a rapid drop in load, which was usually accompanied by clicks stemming from fiber breakage. Samples without fiber damage were kept and those with distinctive and visible fiber damage were excluded from the testing, as exemplified by Figure 8.

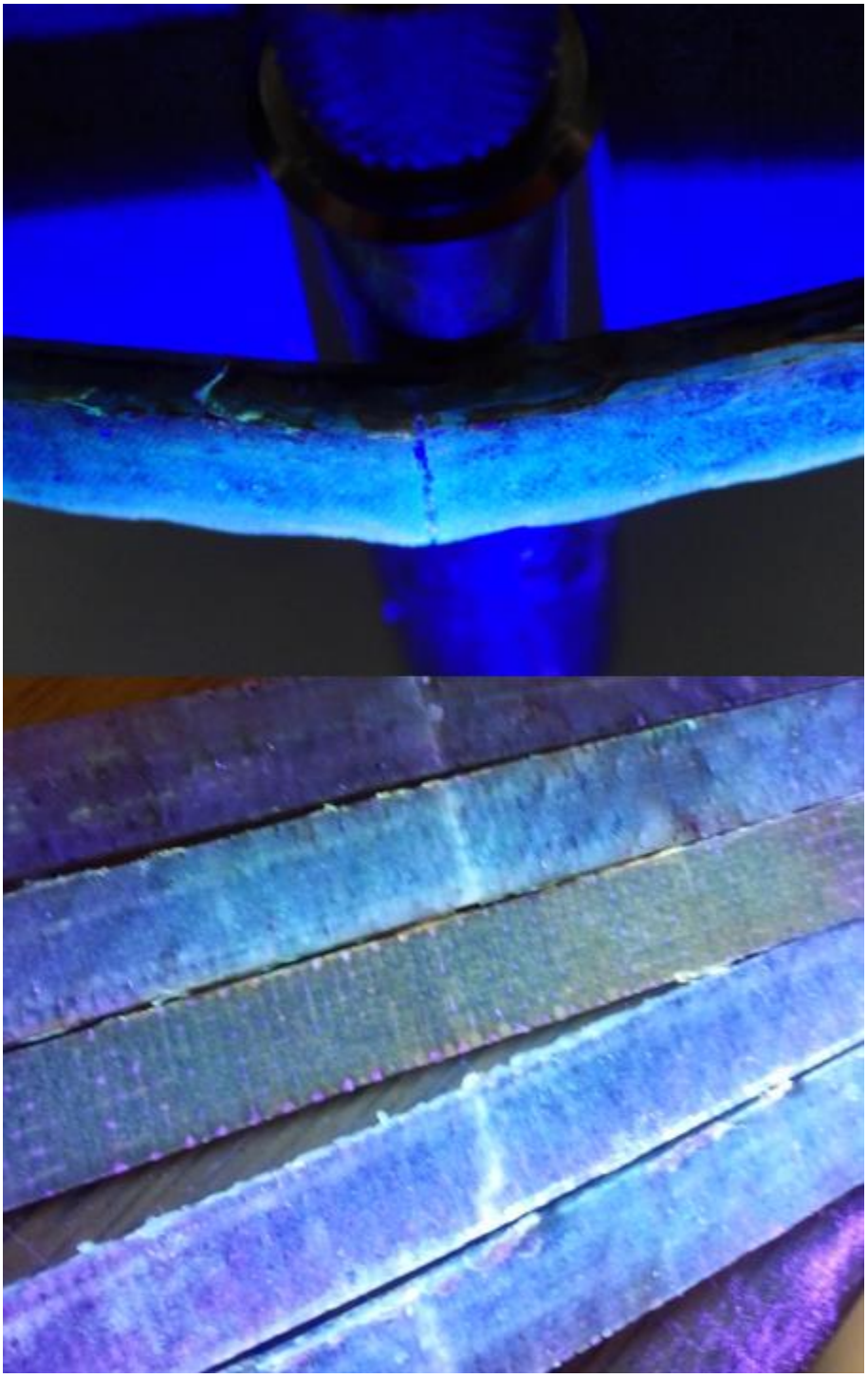

Figure 8: Sample undergoing irreparable fiber dame (Top) and non-fiber damaged (Bottom)

The fiber damaged samples were excluded because with this method fiber damage was irreversible.

To evaluate the copper wire method in a dynamic environment, a three-blade prototype wind turbine was fabricated. One blade was self-healing, and the other two were used as control blades. The blade was designed according to NREL 822 aerofoil profile and molded around a removable 3D printed ABS core. The self-healing blade was molded with two layers of fiberglass and was mounted with a 110 g weight at the end to help induce failure, as shown in Figure 9.

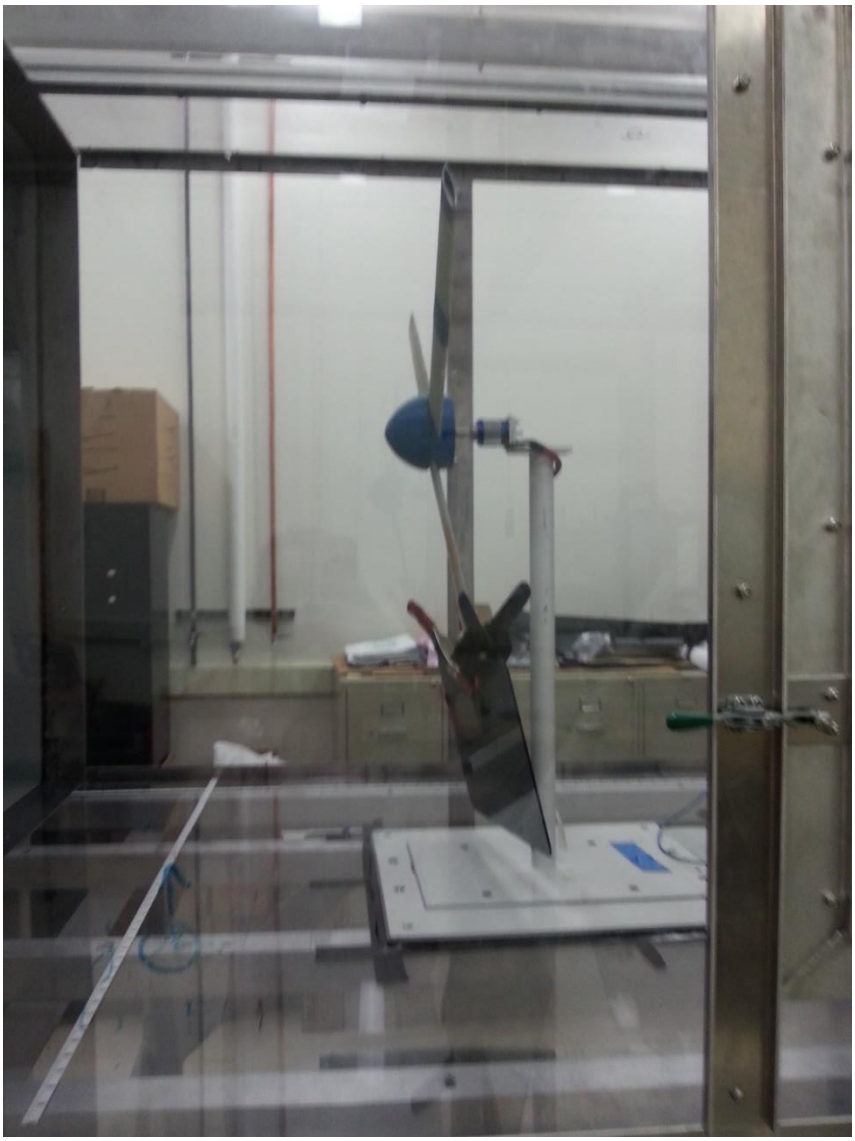

Figure 9: Two-layer self-healing blade subjected to wind tunnel testing.

More than two layers would require additional weight to produce failure and would increase the risk of damaging the wind tunnel upon catastrophic failure. The control blades were molded with six layers to ensure structural strength and stability. A one-directional network was made parallel to the flow at the center of the blade of the turbine blade (spanwise), as shown in Figure 10.

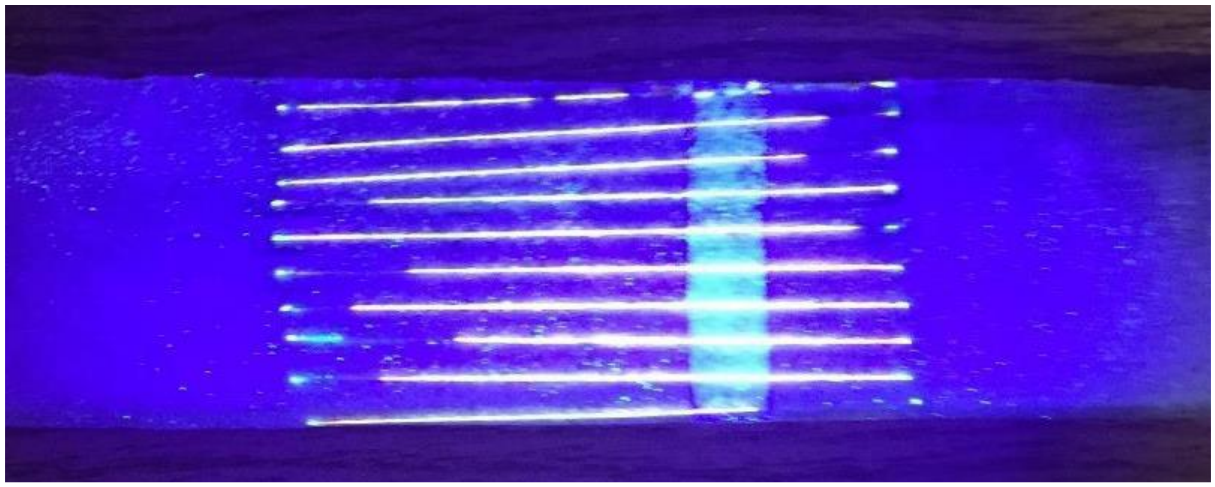

Figure 10: Lengthwise photograph of the FRP self-healing blade under UV light highlighting DCPD filled vascular network at the center of the blade.

DCPD and Grubb's first-generation catalyst was incorporated into the blade using the same method mentioned previously for the FRP sample sheets. The wind turbine prototype was exposed to a wind speed of 16.5 m/s in the test section of the wind tunnel for two hours.

3.2 3D Printed Imprint Layer Method

The 3D printed imprint layer method involves creating a single layer FRP sample with imprinted network henceforward known as the “imprint layer.” The imprinted layer is imbedded into a multilayer sample, replacing a layer of fiberglass. Embedding the imprinted layer into a larger multilayer sample, a single FRP sample with an internal vascular network is created.

3.2.1 VARTM Method Utilizing Glass Mounted Templates

To create self-healing samples, vascular networks are first imprinted into single FRP samples, 3D printed templates. The research presented uses ABS 3D printed grids because of its natural rigidity and compatibility with adhesives. The printed templates were mounted to 127 mm by 178 mm glass

sheets and taped to the glass surface of the VARTM, vacuum-assisted resin transfer molding, apparatus to form the bottom, as shown in Figure 11.

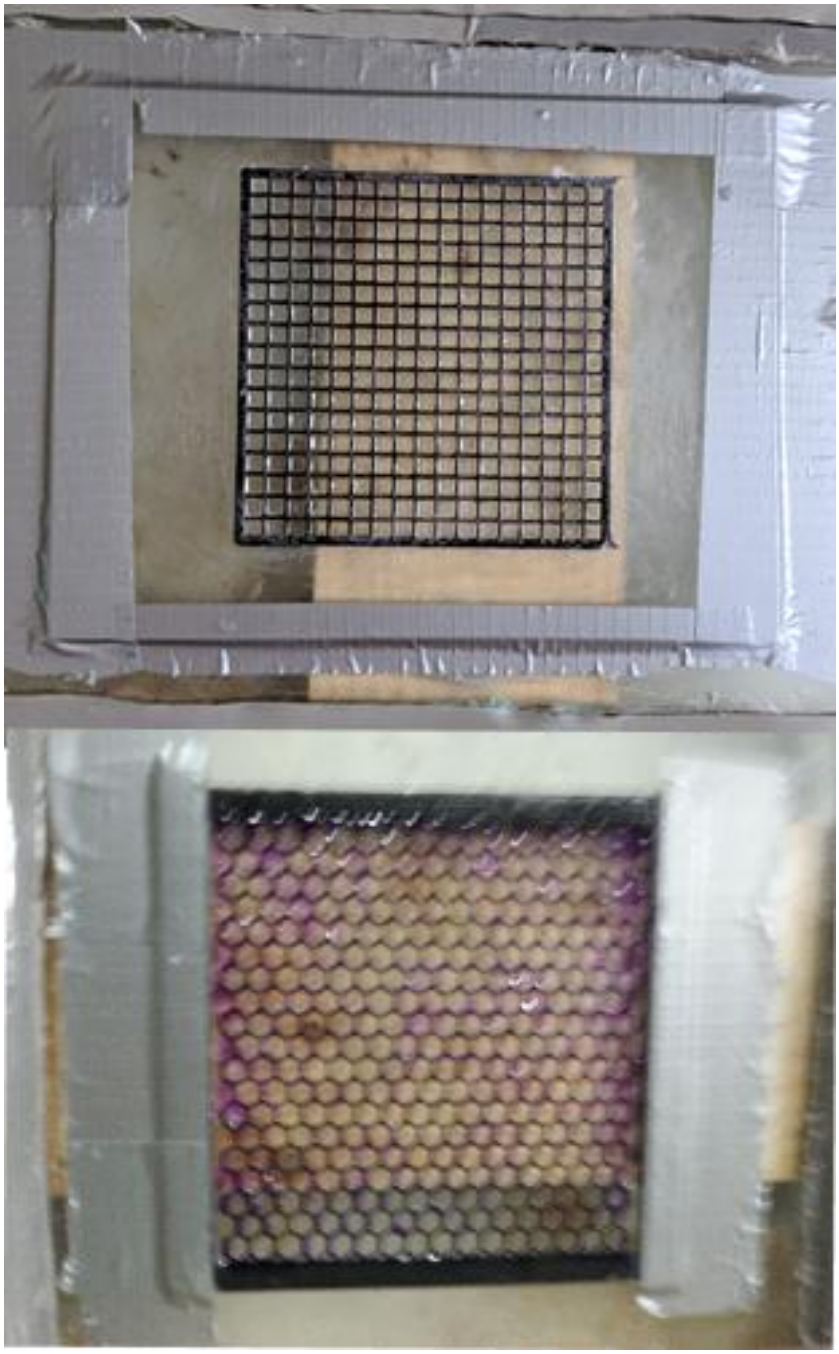

Figure 11: Mounted printed ABS square and hexagonal grid templates before to VARTM.

The bottom glass surface ensures that the epoxy does not flow underneath the template, which makes removal difficult. Two healing sample configurations were used for three of the test

samples, a single-center hexagonal grid network and a single square grid network, as presented in Figure 12 and Table 2.

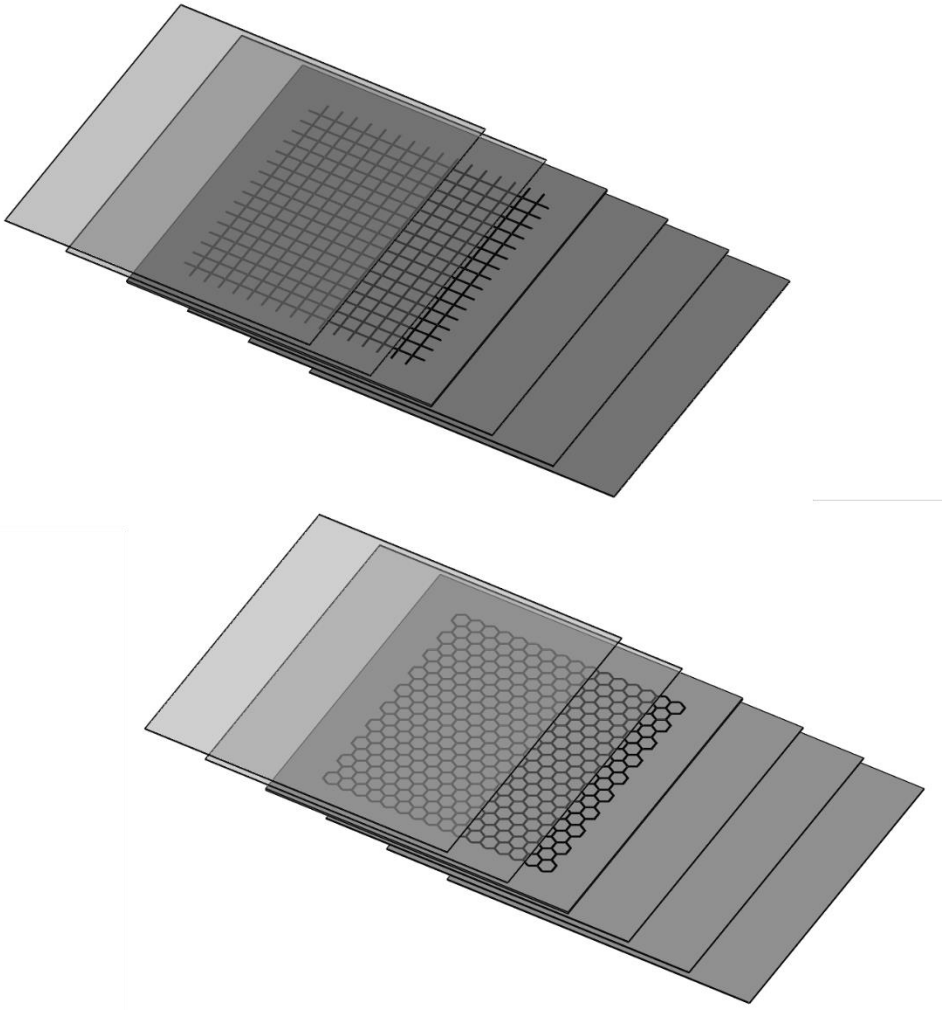

Figure 12: 3D model representations of imprint layers placed between fiberglass sheets. Top, square grid imprint layer as center layer. Bottom, hexagonal grid imprint layer as a center layer.

Table 2: Tabulated samples with imprint layer configuration, use of a catalyst, and location of catalyst.

Sample number	Catalyst Present?	Catalyst Location	Imprint Layer Configuration
Sample 1	No	N/A	N/A
Sample 2	Yes	Imprint Layer	Hexagonal Grid
Sample 3	Yes	Outer Layers	Hexagonal Grid
Sample 4	Yes	Outer Layers	Square Grid

3.2.2 Effects of Grid Geometry and Surface Treatment on FRP Removal from Template

To form the imprint layers the epoxy flows over the glass mounted templates and occupies the volume not occupied to by the 3D printed grid. Once the cured epoxy is removed from the template, the resulting negative is imprinted onto the epoxy layer. Because the epoxy has the potency to bond both chemically and physically precautionary measures were devised.

Initially, rather than mounting the templates to glass the templates wire self-contained, as shown in Figure 13.

Figure 13: Self-contained 3D printed ABS template with paraffin wax coating.

The self-contained templates were able to be created in one step using a 3D printer. The paraffin coated was applied by rubbing paraffin blocks across the top surface in the hope of having the same releasing effect when heated as the wire formed samples. However, even with the additional heat, the templates were severely damage upon the removal of the covering FRP, as shown in Figure 14.

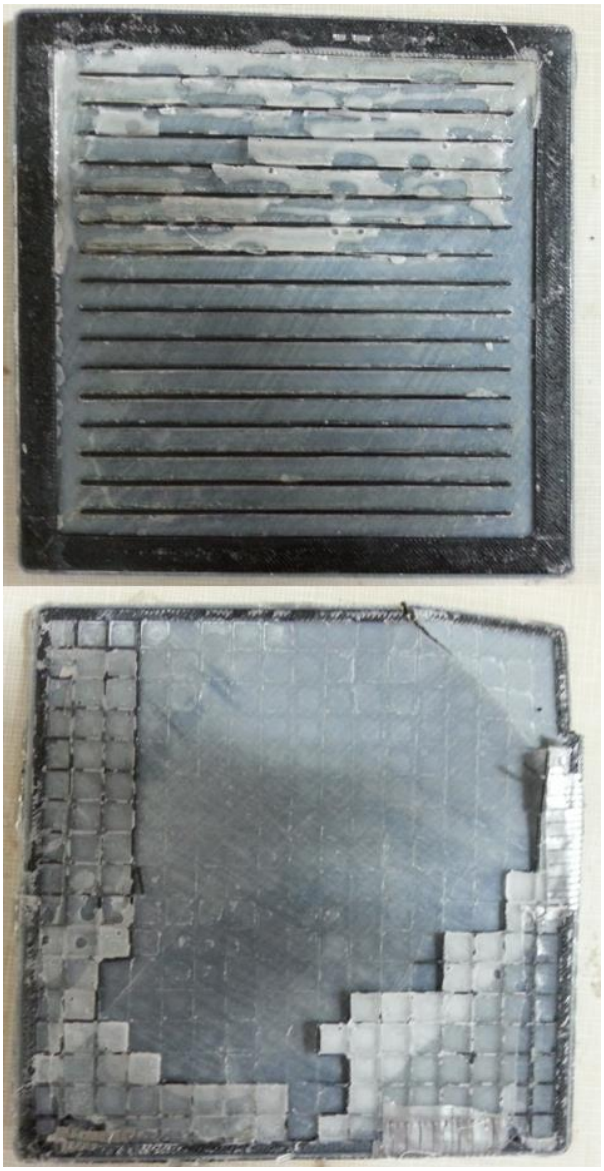

Figure 14: (Top) Vertical line template after FRP removal and (Bottom) Square grid template after FRP removal.

Different lubricants such as WD40, Polytetrafluoroethylene (PTFE), and vegetable oil were trialed with no success. Furthermore, epoxy was evident on the back of the 3D print template removal difficulty. Subsequently, to remove any complications of epoxy penetrating through the

template, the templates without backers were directly mounted to glass. Additionally, instead of a lubricant an adhesive was trialed to produce a sacrificial layer that would come off during the removal of the FRP rather than aid the removal of the FRP itself. A water-soluble adhesive was chosen to aid in clean up and acts as a top coating, as shown in Figure 15.

Figure 15: Square grid coated with water-soluble adhesive to aid in FRP removal.

.

Both square and hexagonal grids were able to be trialed successfully using this method. The hexagonal grid, however, has fewer voids because the flow of epoxy never runs perpendicular to the template as is the case with the square grid templates.

3.2.3 DCPD Imprint Layer Distribution and Seal

Once the VARTM process is completed, the imprint layer is peeled away from the template, and any remaining adhesive is rinsed away, leaving behind a fully formed imprint layer.

After forming the imprint layer, DCPD, Dicyclopentadiene, liquified at 50°C is distributed into the imprinted vascular networks via lab spatula, as shown in Figure 16.

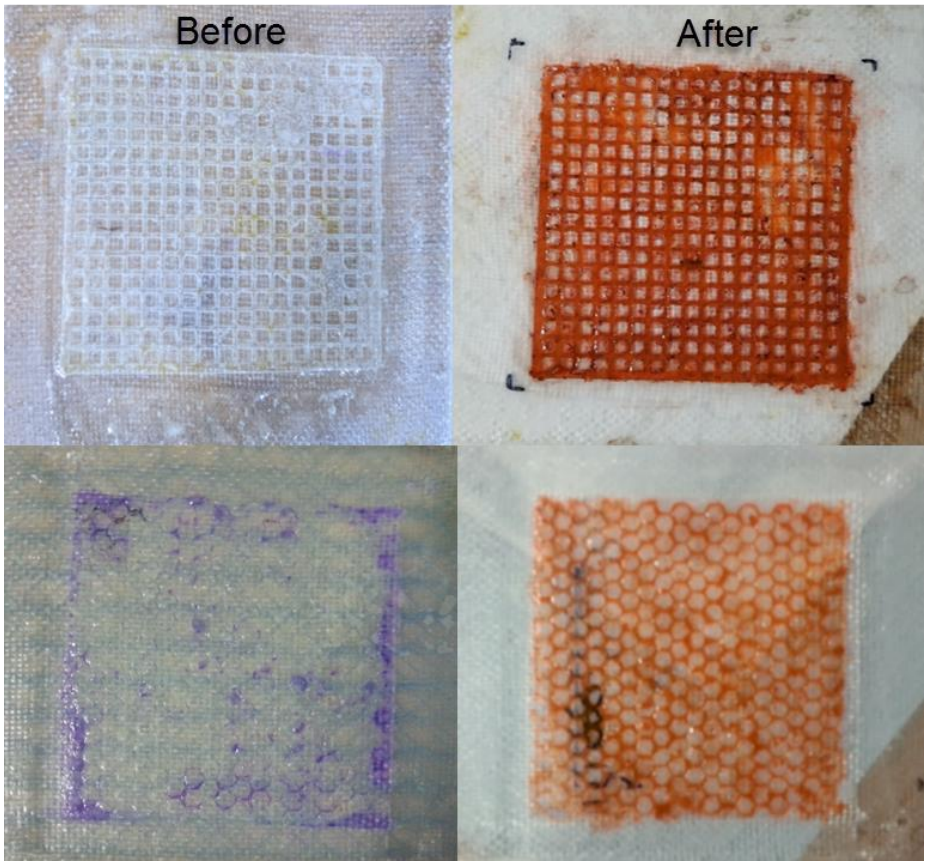

Figure 16: Square grid imprint layer (Top) and hexagonal grid imprint layer (Bottom) before and after DPCD dispersion.

After the DCPD is distributed throughout the imprint layer and cools to room temperature, a sheet of perforated adherent plastic is created to place over the imprinted side, as shown in Figure 17.

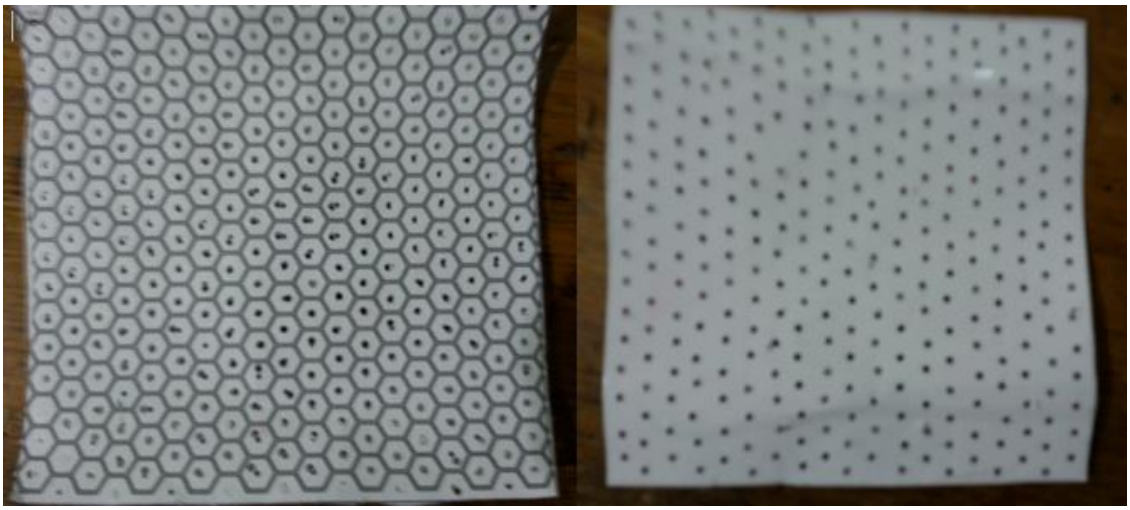

Figure 17: (Left) Template used created a perforated plastic sheet. (Right) Clear perforated adhesive plastic sheet over white backing created by hole punching through the template.

Epoxy cannot be placed directly on top of the DCPD even when the DCPD is in its solid state because the DCPD will dissipate into the epoxy. A thin layer of epoxy is then applied to the plastic sheet is used to seal the DCPD within the imprint layer, as shown in Figure 18.

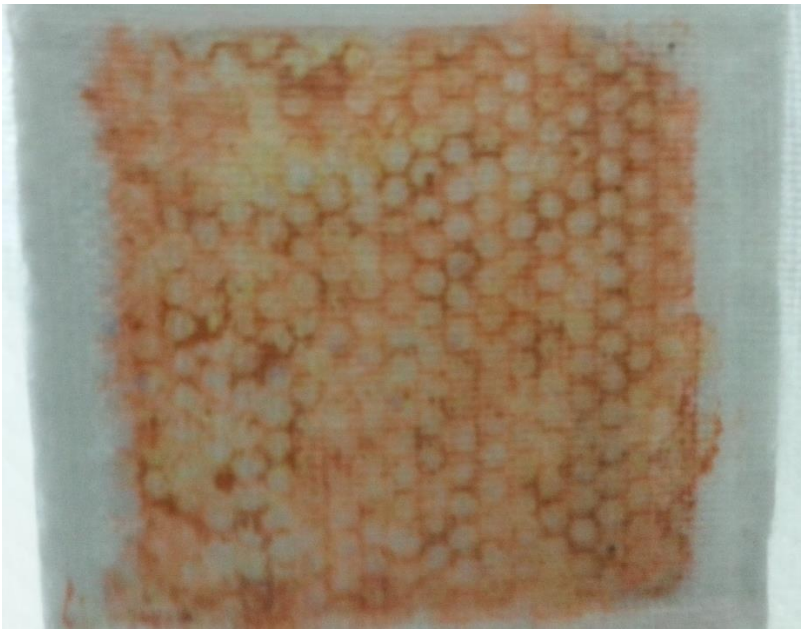

Figure 18: Hexagonal imprint layer covered with a perforated plastic sheet and sealed with epoxy.

The perforation corresponds to the template used so that the holes in the plastic sheet match the areas where only the epoxy is present. When the epoxy seal is applied to the plastic sheet, the holes allow for the epoxy to bond directly to the imprint layer, preventing any delamination that occurs during sample preparation or testing. The epoxy acts as a bonding point when creating the multilayer sample.

The adhesive on the plastic sheeting is to aid in the placement of the sheet only. The perforation and the added epoxy seal create the bond between the imprint layer and the plastic sheet. DCPD outside the imprint vascular network is minimal, and any outlying DCPD may be dispersed into the epoxy. Completed imprint layers were embedded between five glass fiber sheets, as shown in Figure *19*.

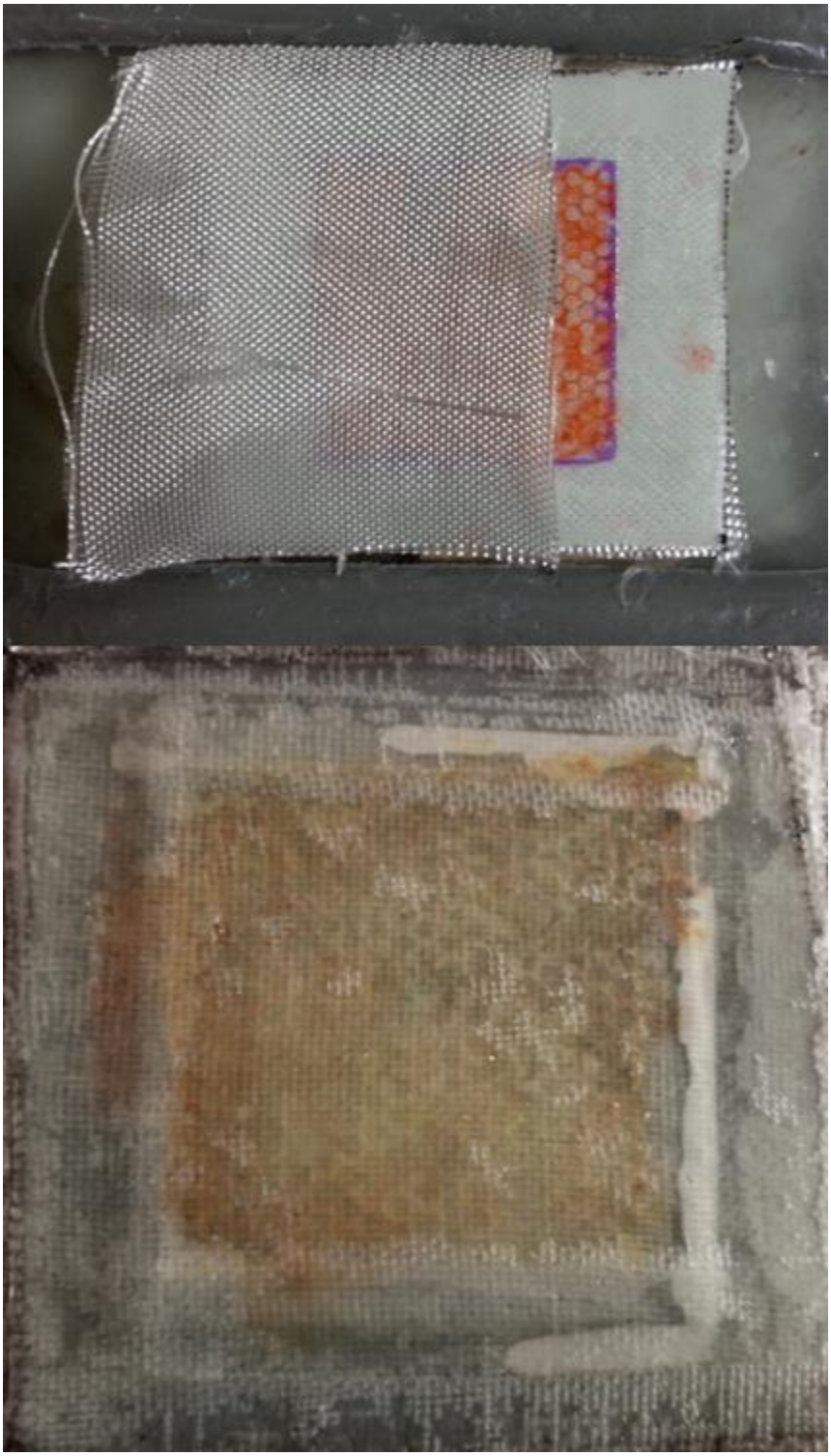

Figure 19*: DCPD filled imprint layer placed in between fiberglass sheets. Before (Top) and after VARTM (Bottom)*

To track the flow of the DCPD within the multilayer sample, the fluorescent dye was added. During the creation of the multilayer sample, no traces of dye were evident downstream, as shown in Figure 20.

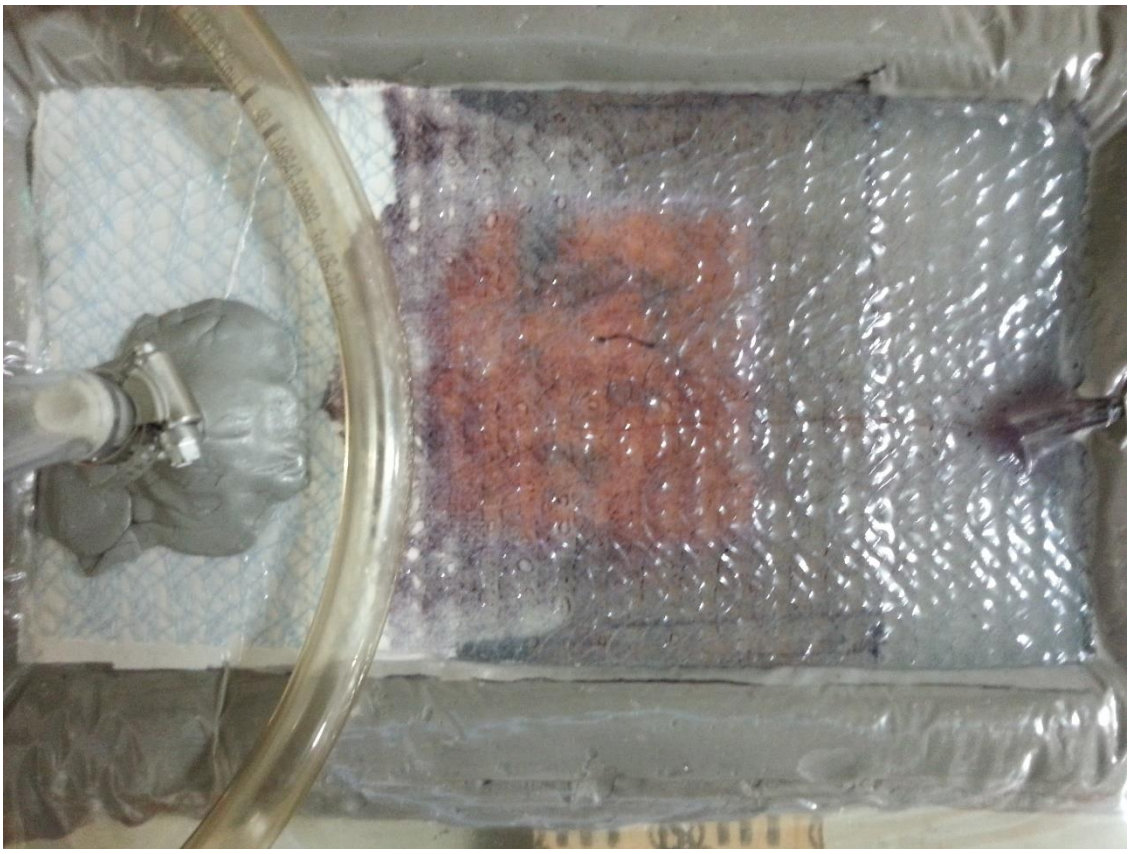

Figure 20: Multi-layer sample with DCPD filled imprint layer during VARTM. Lack of fluorescent DCPD streaks leading from sample demonstrate the security of the epoxy seal on the imprint layer.

.

To heal the multilayer sample, two variations on the placement of Grubbs' first-generation catalyst henceforward called catalyst were trialed. For one variation catalyst was interspersed

into the imprint layer uncured resin before running the VARTM process, and for the second variation catalyst was dispersed into the epoxy of the outer layers.

3.2.4 Imprinted Vascular Network Sample Test Preparation

Samples 1-4 were cut into 12.7 mm strips for flexural testing. The exposed openings of the networks were sealed using a standard adhesive. The prepared samples were subjected to three-point bending flexural tests, samples tested once, referred to as unhealed samples and samples tested twice, before and after healing, are referred to as healed samples. The samples were tested at room temperature and then later heated at 50°C for two minutes after testing. The temperature of 50° C was chosen over 120° C as a precautionary measure. 50° C was judged suitably high enough to liquefy the DCPD within and per Kessler et al. [18] catalyst exposed to temperatures above 80° for extended periods will degrade the catalyst activity. For previous samples, it is unlikely that two minutes was enough to cause significant degradation. The unhealed samples after testing were placed flat below a dead weight for 24 hours. According to Kessler et al. [13], the healing time is dependent on local catalyst concentration and that longer healing times (>1500 min) provided optimal results so, the unhealed samples were subjected to another round of bending tests after a healing time of 24 hours.

Sample strength was determined through three-point flexural testing. Three-point flexural tests were performed while maintaining a 32:1 span to sample thickness ratio and with a cross-head rate of 3.81 mm/min. The rate was increased from the cross-head rate of 1.27 mm/min used in previous research for wire formed and borosilicate tube networks to reduce testing time. Elanchezhian et al. [19] investigated the effects of strain rate and thickness on glass fiber reinforced epoxy composites. Their research showed that with strain rates of 1.5 mm/min to 2.5

mm/min, the glass-reinforced epoxy samples proved strain insensitive. The stopping point for the flexural tests was marked by the continued deflection of the samples without an increase in load. Samples without fiber damage were kept, and those with distinctive and visible fiber damage were excluded from the testing.

CHAPTER 4: RESULTS

4.1 Wire Formed Vascular Network Testing Results

4.1.1 Evaluating Storage Efficiency Across Methods

Until now, microcapsules and tubes/fibers were the primary methods to store and transport self-healing agents. To compare the wire formed network's ability to store healing agent versus the ability of other methods, the amount of healing agent available versus the total volume occupied by the vessel housing the healing agent, the storage efficiency, was calculated. Examining the study done by White et al. [8], for a .2 mm diameter spherical microcapsule with a .01 mm wall thickness, the inner to total volume ratio, storage efficiency was 75%. An additional consideration is warranted due to the isolation of the microcapsules. By localizing the healing agent, samples are limited to healing a single damage event per site and require the rupture of multiple microcapsules for more massive fractures. Considering the study done by Motuku et al. [12], for a 1.15 mm outer diameter borosilicate pipette with a 0.06 mm wall thickness, the storage efficiency was 64%. In the study by Matt et al. [13] for a .5 mm outer diameter borosilicate pipette with a .125 mm wall thickness, the corresponding storage efficiency was 25%. In comparison, the networks produced in this study provide an inner to total volume ratio of 1:1 equates to a 100% storage efficiency, a four-times improvement over the .5 mm outer diameter pipettes as illustrated by Figure 21.

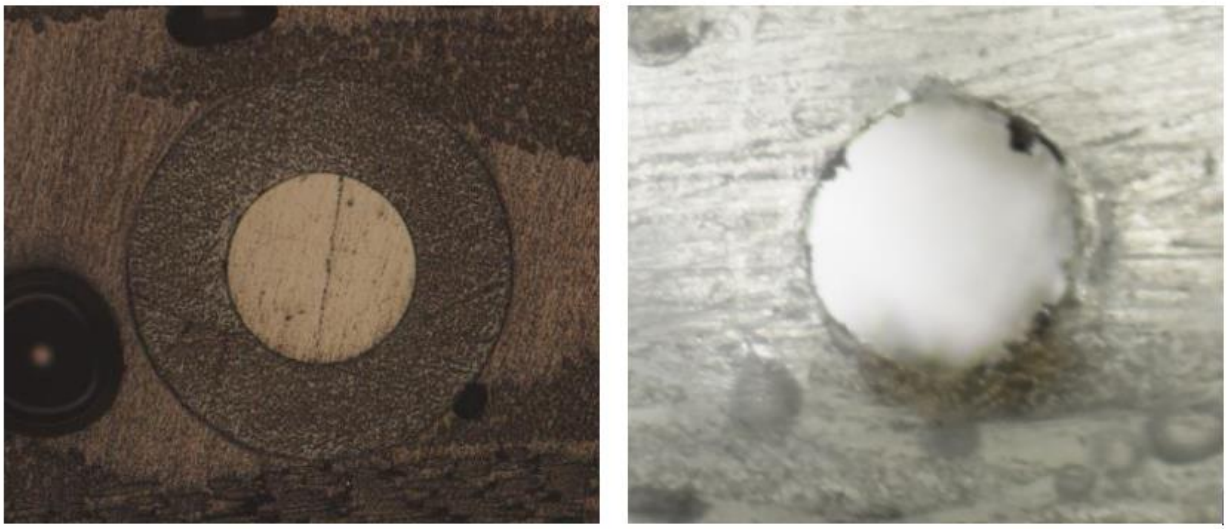

Figure 21: For optical examination, the samples were polished by 200, 1000, and 2000 grit silicon carbide emery papers progressively. Micrographs were taken using a stereo-microscope for review. Borosilicate pipette with 25% storage efficiency (Left: [10]). Cavity produced by copper wire with 100% storage efficiency (Right).

In pursuits to create a self-healing FRP that provides 100% storage efficiency, various methods were trialed. Bare metal wires were embedded in the epoxy matrix with hopes to form cavities after extraction. However, the sample epoxy firmly fixed the wires into place. The thread was trialed and embedded in the epoxy matrix, but both bare and wax coated thread even left residual thread strands in the sample. Low melt plastic was also used, but the melt temperature surpassed the operating temperature of the used epoxy rendering it useless. Coated nickel-chromium wires were embedded but tended to curl during layout and break upon extraction. Coated copper wire as the stronger and stiffer material was chosen of over nickel-chromium wire to help avoid wire breakage upon retrieval and to assist in the wire straightening and network layout process.

4.1.2 Flexural Strength and Percent Recovery Comparisons Between Wire Formed Vascular Network Configurations

As mentioned, the flexural tests were run according to composite flexural test standard ASTM D7264, the sample width was 12.7 mm, the sample thickness ranged from 1.9-2.5 mm, and a sample span to thickness ratio of 32:1 was maintained. Less than 40% of samples were able to heal correctly and which was mostly caused by sample overload and critical glass fiber damage is beyond the ability of DCPD and Grubbs' first-generation catalyst to heal. Due to the low sample size, the qualitative results may fluctuate with further testing. However, the overall sample performance hierarchy is expected to uphold. The samples that were assessed as unable to heal flexed freely at the center after 24 hours and were not subjected to another round of flexural testing. Of the samples that successfully healed, approximately 80% of their strength on average was recovered as indicated in Figure 22, Figure 23, and *Table 3*. Sample 4 did not regain rigidity after 24 hours and so was only tested once.

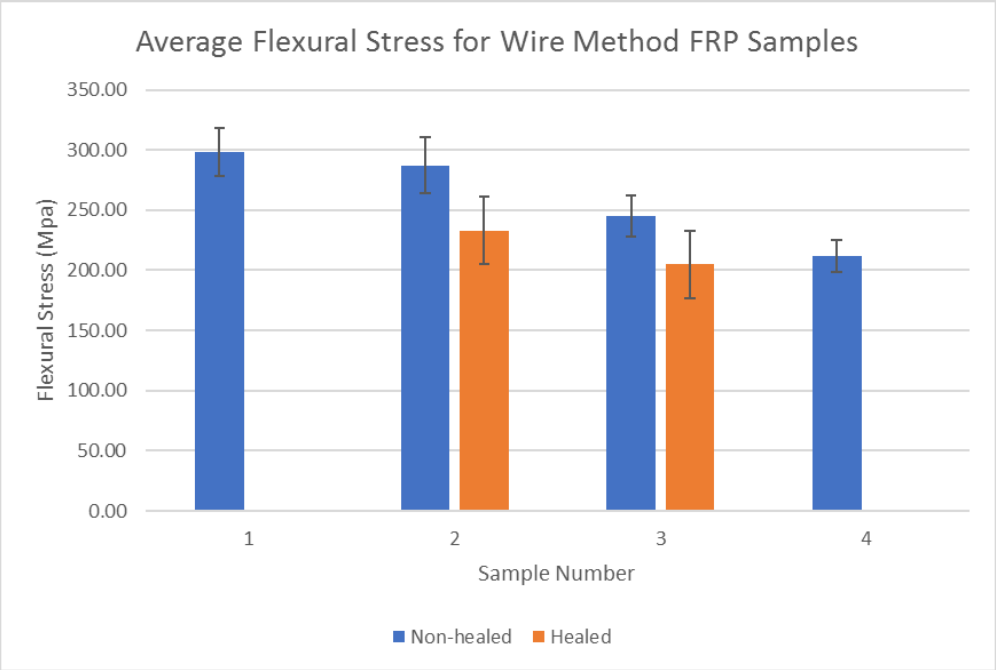

Figure 22: Flexural testing results for FRP samples 1-4, showing sample 2 with the highest original and recovered flexural strength of the test samples.

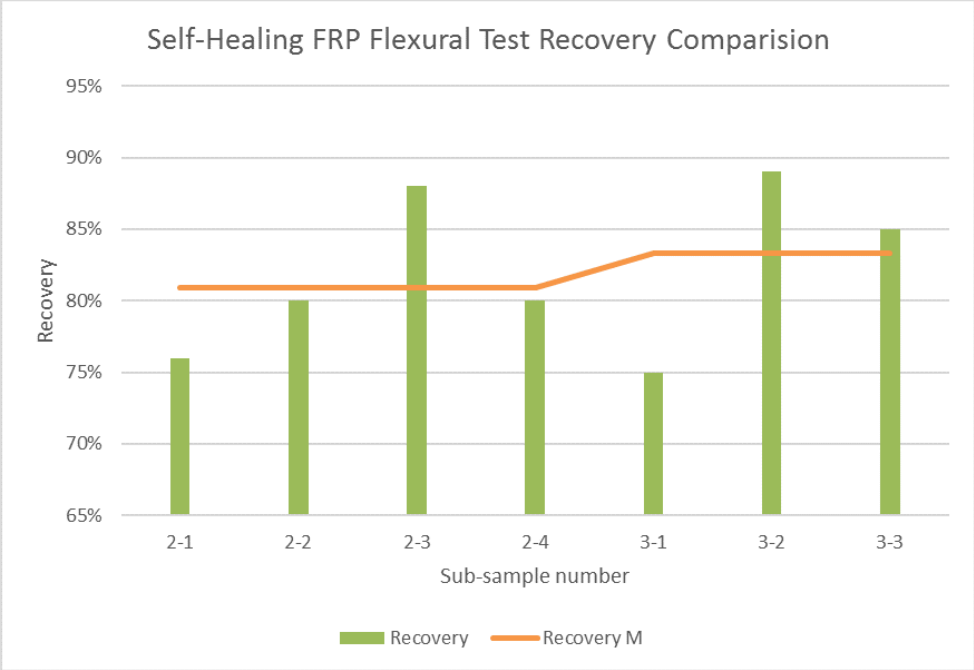

Figure 23: Recovery analysis for flexural tested FRP self-healing samples 2 and 3, showing sample 3 with marginally higher recovery rate in comparison to sample 2.

Table 3: Tabulated samples with healed and non-healed flexural strengths with corresponding recovery statistics.

Samples	Non-healed	Healed	Recovery	Non-healed **Mean**	Healed **Mean**	Recovery **Mean**	Non-healed **Std. Deviation**	Healed **Std. Deviation**	Recovery **Std. Deviation**
	(MPa)	(MPa)	(%)	(MPa)	(MPa)	(%)	(MPa)	(MPa)	(%)
1	282.38	N/A	N/A	298.42	N/A	N/A	20.00	N/A	N/A
	314.96								
	290.39								
	330.35								
	273.52								
	289.23								
	282.87								
	323.67								
2	246.85	187.49	76%	287.18	233.08	80.92%	23.32	28.33	4.25%
	300.45	241.84	80%						
	302.58	265.25	88%						
	298.84	237.75	80%						
3	223.87	168.85	75%	244.94	205.04	83.32%	17.30	28.08	5.78%
	266.25	237.29	89%						
	244.69	208.97	85%						
4	220.56	N/A	N/A	211.95	N/A	N/A	13.30	N/A	N/A
	212.68	N/A	N/A						
	190.13	N/A	N/A						
	224.45	N/A	N/A						

Of the self-healing capable samples, sample two had the highest yield stress values with an average non-healed stress of 287.18 MPa. Additionally, sample two had average non-healed and healed yield stresses 17.25% and 13.68% higher than that of sample three. Sample three, however, had an average recovery of 2.97% higher than sample two. Based on yield stress and recovery statistics, the value derived from the increase in recovery is diminished by the lower

yield stress. Sample four testing resulted in non-healed yield stress 35.49% lower than sample three. A recovery percentage greater than 83.32% would be necessary for the use of this network to be justifiable.

4.1.3 Wire Formed Sample Healing Agent Transport During Three-Point Bending Testing

To observe the transport process of the healing agent throughout testing, UV light reactive dye incorporated samples were examined under UV light. During the course of testing, the sample underwent four stages as depicted by Figure 24. For the initial stage, the sample is without load. In the second stage, the sample is under load but not fully yielding. Small-scale cracking begins to occur, and DCPD begins to release. During the third stage, large-scale fracturing occurs at the yield point of the sample and the DCPD flow increases. At the the fourth stage, the load is removed, and the sample is allowed to relax with unused healing agent remaining for future crack events.

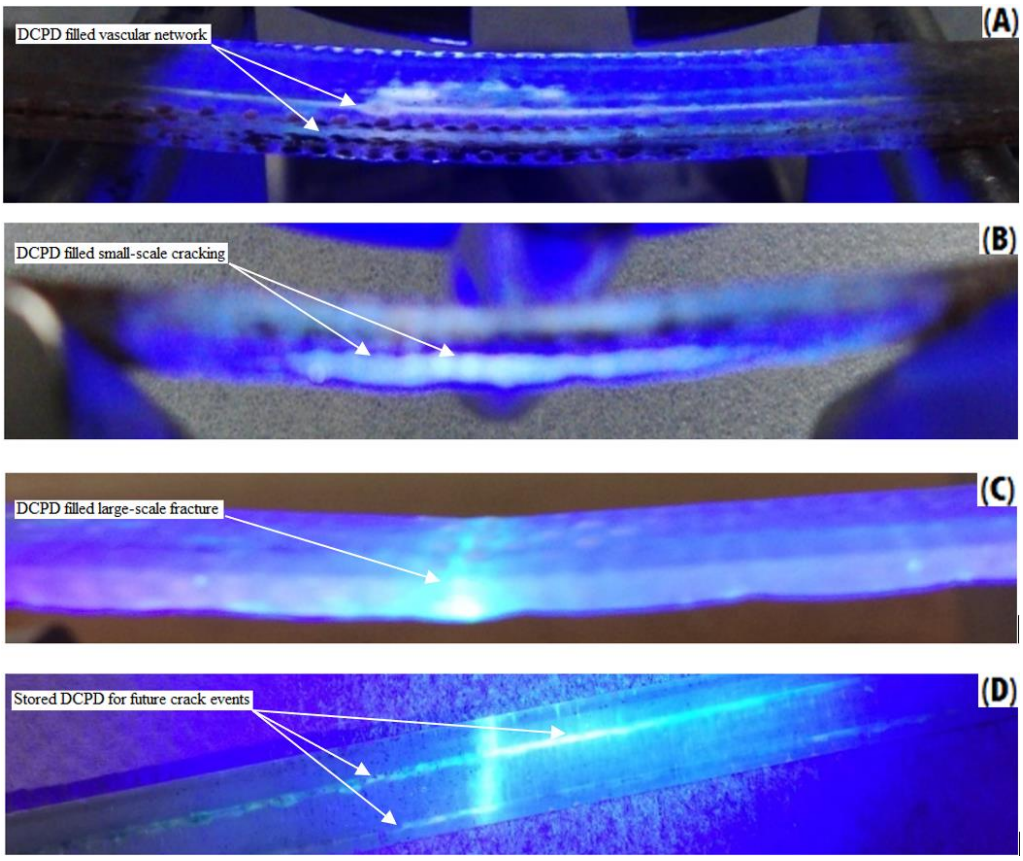

Figure 24: Four test stages that samples filled with fluorescent healing agent under UV light underwent during flexural testing: (A), Initial unloaded stage; (B), pre-yield stage with small-scale cracking releasing DCPD; (C), large-scale fracture and sample yield stage resulting in further release of DCPD; (D), final load removal stage.

As the samples themselves act as the vessels for the healing agent, any micro cracks that form and penetrate the healing network at any point were immediately filled. For the borosilicate pipettes used in the previously mentioned studies, the crack propagation had not only reached the tubes but also there must be a load present high enough to fracture the tubes at that location. In those cases, care in preparation must be taken so that the strength of the tubes is not too low relative to the composite matrix to prevent the decrease of the overall strength of the composite and not high as not fracture during sample crack propagation.

4.1.4 Wind Tunnel Testing of The Prototype Composite Wind Turbine Utilizing Wire Formed Vascular Networks

To evaluate how effectively the wire formed network would heal an actual wind turbine blade, a FRP fabricated wind turbine was installed inside of a wind tunnel producing a wind speed of 16.5 m/s for two hours. An external 110 g weight was mounted to the end of the test blade to increase the bending stress at the network site to help induce failure, as shown in Figure 25.

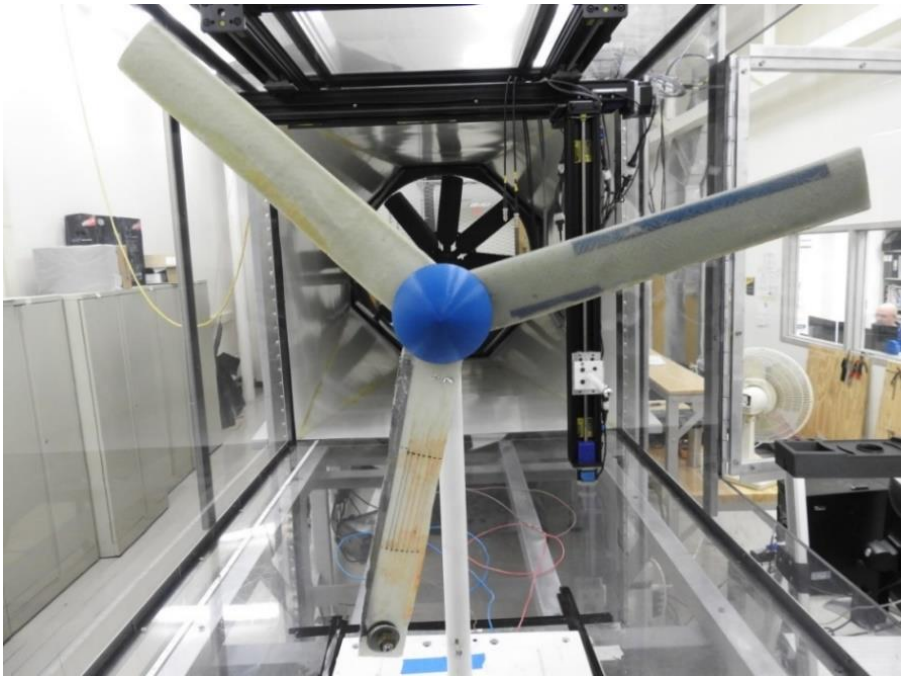

Figure 25: Fabricated wind turbine installed in a wind tunnel producing a 16.5 m/s wind speed. The test blade is shown oriented downward with mounted 110 g weight to increase the load and induce failure.

After the two hours test duration, visible transport of the healing agent in the test blade was observed, as shown in Figure 26.

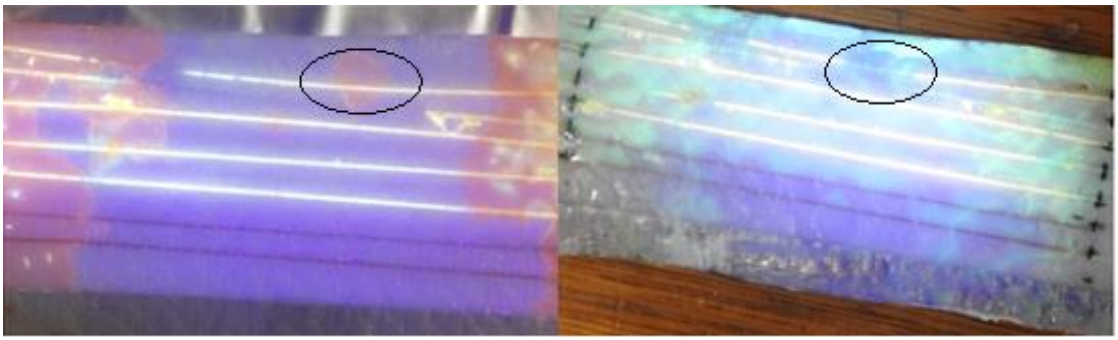

Figure 26: Photographs of self-healing turbine blade under UV light. Photograph of test blade before testing showing the presence of the healing agent(Left). Photograph of test blade after testing revealing healing agent transport from one cavity (Right).

4.1.5 Raman Spectroscopy Analysis to Determine Percentage DCPD Polymerization

At the cost of the sample, flexural testing was performed on healed and non-healed samples to determine their percent recovery. When non-destructive methods are more desirable, Raman spectroscopy provides a way to analyze and monitor sample recovery [20]. Due to blade curvature and profile, flexural a Horiba XploRA PLUS Raman microscope was used to examine the extent of the blade's recovery.

For DCPD to polymerize and create the thermoset polydicyclopentadiene (PDCPD), the DCPD first reacts with the Grubb's first-generation catalyst to initiate ring-opening metathesis polymerization (ROMP) [21]. The ROMP process then promotes polymer cross-linking to produce the thermoset, PDCPD, as shown in Figure 27.

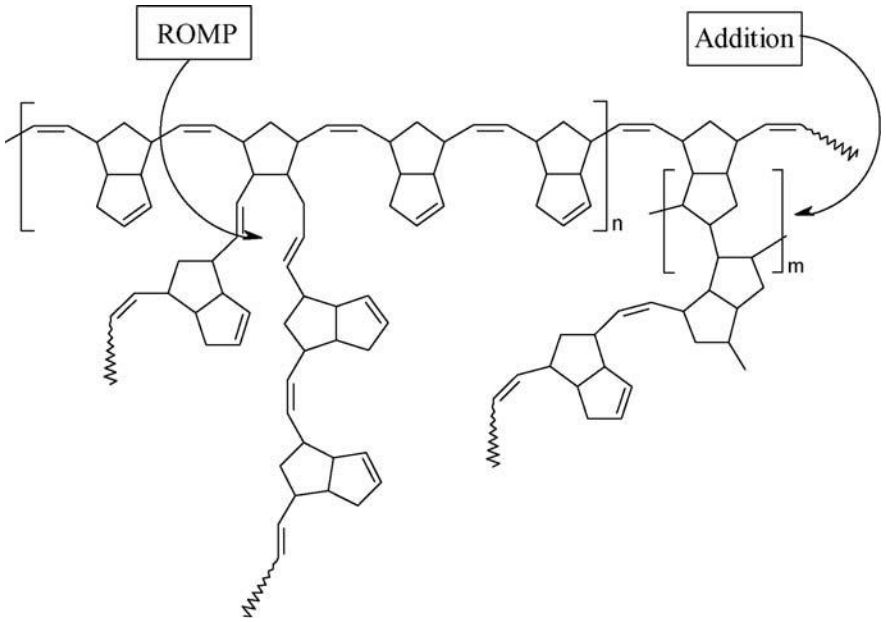

Figure 27: A bond diagram showing DCPD responding to ROMP reaction to crosslink and create PDCPD [21].

Raman spectroscopy monitors the polymerization process by observing the wavenumber and corresponding intensity. The typical Raman spectra of DCPD's polymerization to PDCPD is depicted in Figure 28.

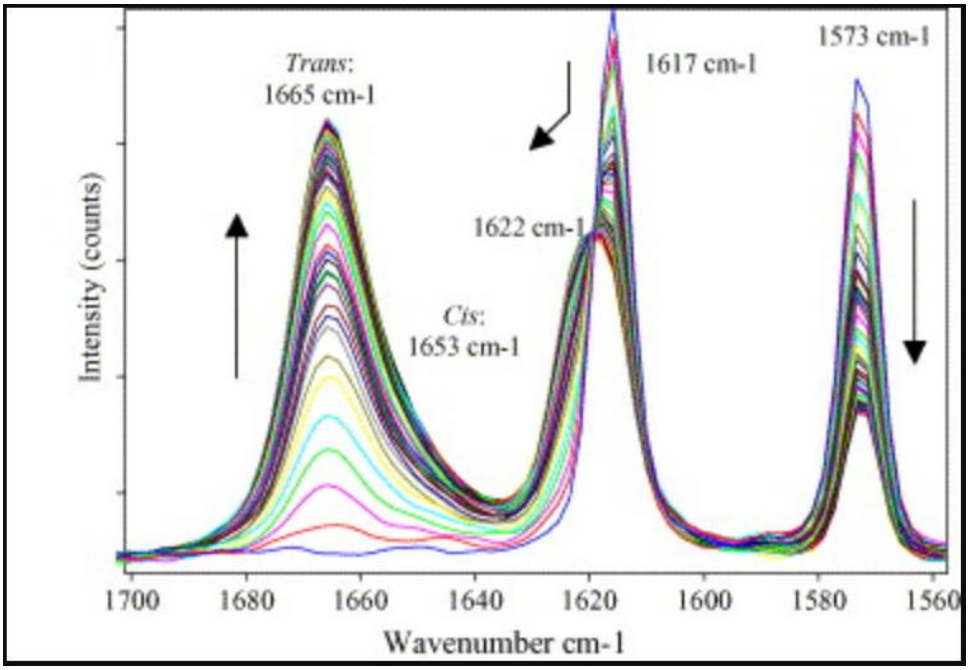

Figure 28: Raman spectra are depicting the band changes of DCPD during ROMP reaction [21].

The five bands that are of interest for this study: the 1573 cm^{-1} band, correlates to the percentage of DCPD in the system; the 1617 cm^{-1} band, corresponds to the ring-opening before crosslinking; the 1622 cm^{-1} band relates the crosslinking action of DCPD to form PDCPD; the 1653 cm^{-1}. Moreover, the 1665 cm^{-1} band equates to the percentage of fully formed PDCPD [21]. After 24 hours of heal time, Raman spectroscopy was performed at the crack location on the test blade to yield the Raman spectra shown in Figure 29.

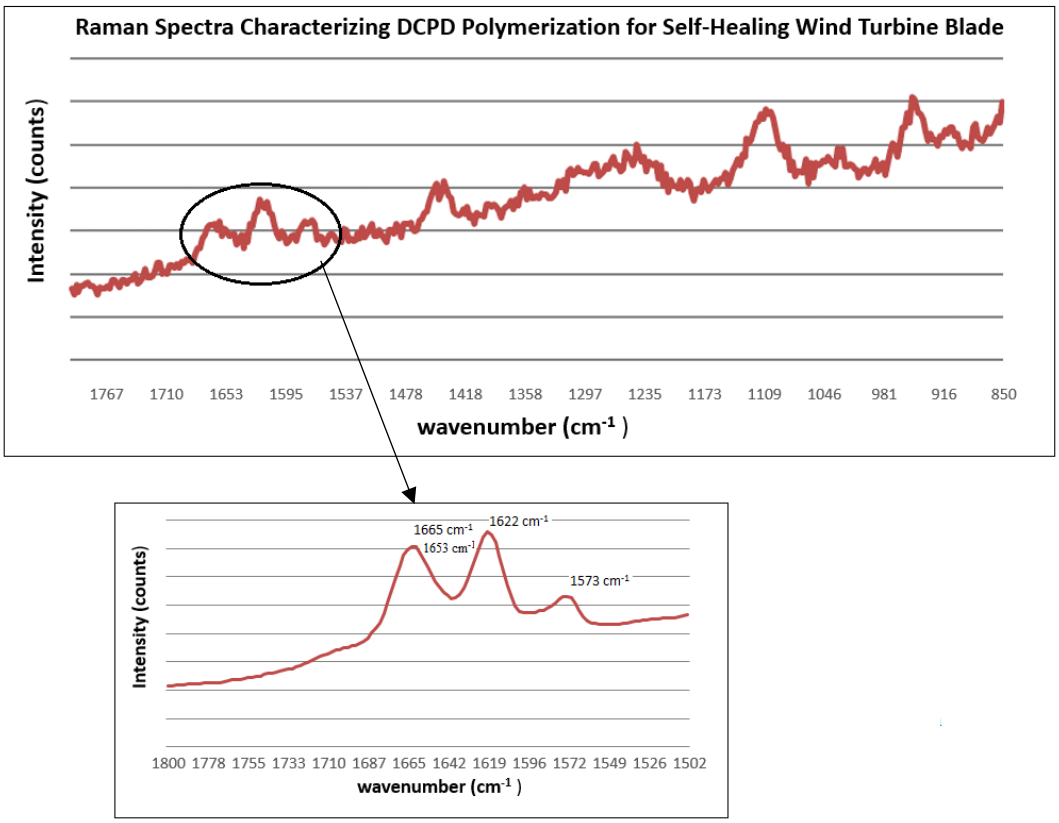

Figure 29: Raman spectra taken at the crack of the test blade highlighting the bands present after 24 hours of self-healing.

The focused portion of the Raman spectra highlights four of the five bands present after the 24 hour healing time. The right side of the red circle can be ascribed to the epoxy matrix [22]. Based on the Raman spectra, the blade sample was able to successfully heal as indicated by the relatively high intensity of the 1622 cm^{-1}, 1653 $cm^{-1,}$ and 1665 cm^{-1} bands compared to the 1573 cm^{-1} band. From the band intensity values, the total recovery for the test blade was estimated to be 84% which correlates with the flexural testing recovery values.

4.2 3D Printed Imprint Method Vascular Network Test Results

4.2.1 Flexural Strength And Percent Recovery Comparisions Between Imprint Layer Network Configurations

Of the imprint samples made for testing, 100% were able to heal successfully with recovery rates averaging over 175%. The average strength nearly doubled after recovery, as shown in Figure 30, Figure 31, and Table 4.

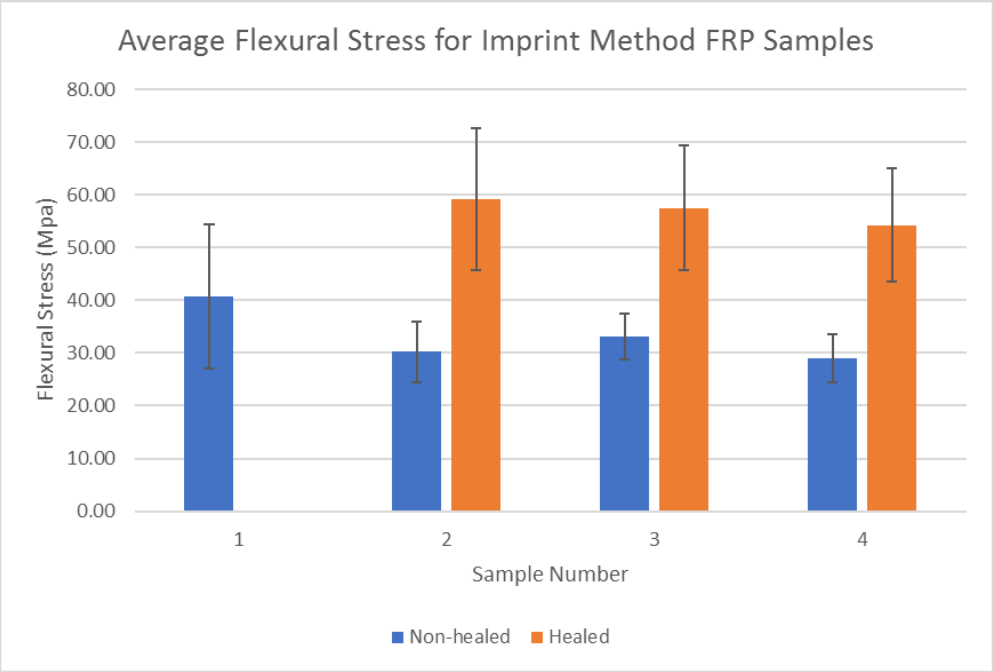

Figure 30: Flexural testing results for FRP samples 1-4, showing sample 2 with the highest original and recovered flexural strength of the test samples.

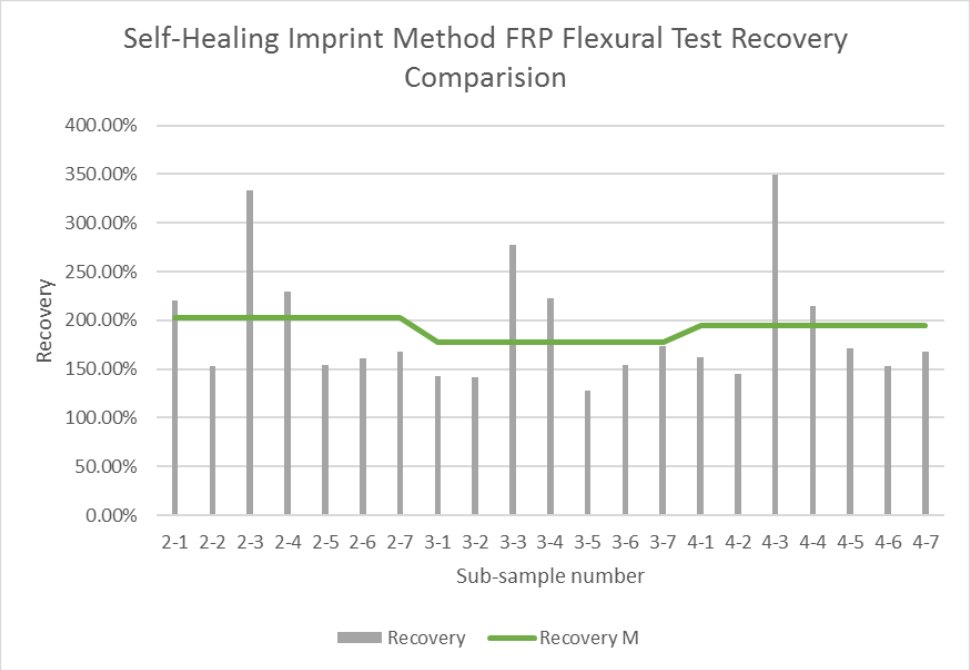

Figure 31: Recovery analysis for flexural tested FRP self-healing samples 2, 3, and 4 showing sample 2 with marginally higher recovery rate in comparison to sample 4.

Table 4: Tabulated samples with healed and non-healed flexural strengths with corresponding recovery statistics.

Samples	Non-healed	Healed	Recovery	Non-healed **Mean**	Healed **Mean**	Recovery **Mean**	Non-healed **Std. Deviation**	Healed **Std. Deviation**	Recovery **Std. Deviation**
	(MPa)	(MPa)	(%)	(MPa)	(MPa)	(%)	(MPa)	(MPa)	(%)
	59.45								
	50.34								
	28.34								
	23.10								
1	61.30	N/A	N/A	40.71	N/A	N/A	13.66718	N/A	N/A
	31.35								
	30.07								
	49.83								
	32.58								
	19.83	43.72	220.48%						
	38.88	59.57	153.21%						
	25.38	84.62	333.41%						
2	31.30	71.99	230.00%	30.20	59.24	202.89%	5.66	13.46	60.84%
	32.01	49.27	153.90%						
	30.13	48.47	160.87%						
	33.87	57.02	168.35%						
	30.95	44.15	142.68%						
	41.99	59.57	141.86%						
	27.41	76.15	277.85%						
3	31.61	70.55	223.17%	33.12	57.45	177.38%	4.28	11.83	50.15%
	34.57	44.34	128.25%						
	30.73	47.50	154.56%						
	34.55	59.87	173.30%						
	25.93	41.97	161.84%						
	37.71	54.80	145.32%						
	21.83	76.15	348.92%						
4	28.48	61.19	214.84%	28.97	54.27	194.84%	4.55	10.68	66.20%
	27.53	47.30	171.80%						
	30.13	46.04	152.82%						
	31.16	52.46	168.35%						

Non-healed hexagonal samples experienced an average non-healed and healed stresses of 30.20 MPa and 59.24MPa and 33.12MPa and 57.45MPa for imprint and non-imprint layer catalyst samples respectfully. The resulting recovery for the imprint layer catalyst sample was 202.89% and the non-imprint layer catalyst sample was 177.38%. The grid samples had an average non-healed and healed stresses of 28.97 MPa and 54.27 MPa. The control sample had a non-healed stress of 40.71.

Healed samples experience an increase in strength because before healing a percentage of the structure is occupied by the non-load bearing DCPD. After cracking occurs releasing the DCPD to react with the catalyst the thermoset PDCPD, forms. The resulting PDCPD is approximately 50% as strong as the bonding epoxy [23].

For flexural testing, the span to sample thickness ratio is 32:1. The samples created using the wire method were 2 mm in thickness and the samples created in this experiment were 3 mm thickness resulting in a larger span. Thinner and more flexible samples combined with a larger span meant lower loads for an equivalent amount of deflection explaining the difference in stress values for the two methods. The stopping criteria are independent of the sample dimensions, and the same amount of damage is enacted for each sample. Therefore, the percent recovery data for each sample set creates a valid comparison. Both the wire method and imprint method use the same materials and have the same storage efficiency so one could reasonably expect that with equivalent span and sample thickness the average maximum stress would be similar between methods.

4.2.2 Imprint Layer Embedded Sample Healing Agent Transport During Three-Point Bending Testing

The high recovery percentage can be contributed to two factors. There is a higher quantity of DCPD located within the sample because of the interconnected grid configurations. The printed grids create one interconnected network to supply DCPD versus the wire method where reservoirs were separated. The storage and transport modes of the hexagonal grid are shown in Figure 32.

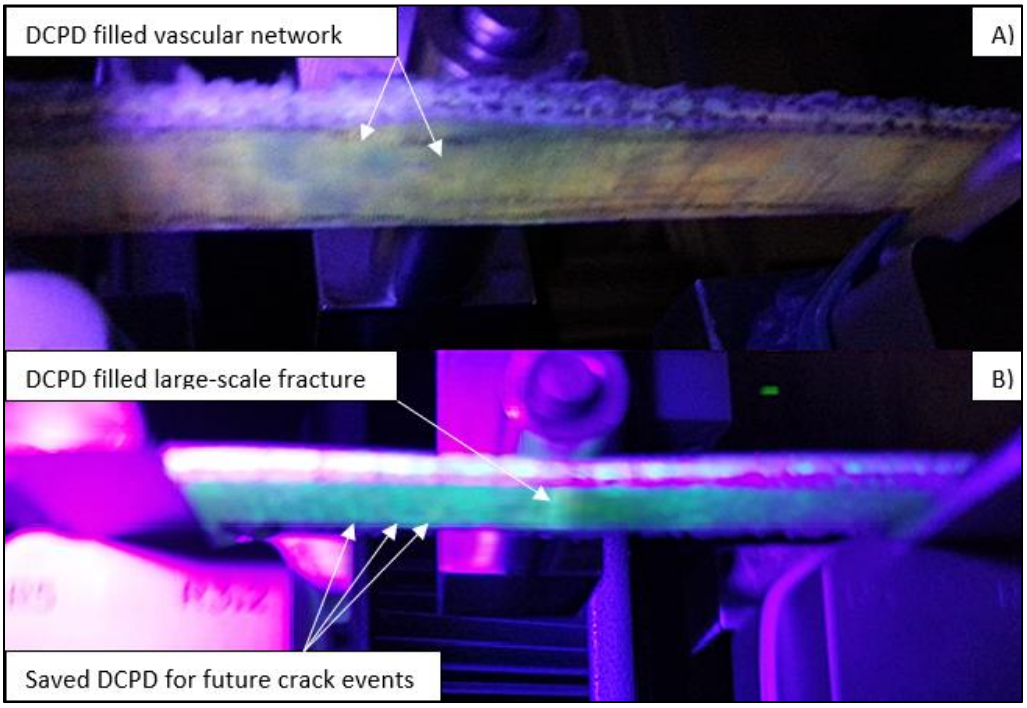

Figure 32: Two test stages that samples filled with the fluorescent healing agent under UV light underwent during flexural testing: (A) Initial unloaded stage, and (B) Healed unloaded stage.

Comparing the hexagonal grid to the square grid there is little difference when examining the flexural testing results. However, the hexagonal grid has DCPD in three directions enabling greater access to DCPD during cracking events that occur in any direction versus the square grid

only being able to account for two directions. Furthermore, the hexagonal shape is optimal for VARTM flow because none of the template used for imprinting runs perpendicular to the flow preventing air pockets and aiding release. Ease of creating square versus hexagonal grid samples is demonstrated by the state of the templates after removing the created imprint layer.

4.2.3 Imprint Layer Catalyst Sample Recovery and Outer Layer Catalyst Sample Recovery Results

Based on flexural testing results catalyst in the imprint layer versus the entire multilayer sample had little effect on percent recovery. The average maximum stress percent recovery for the hexagonal samples were 202.89% and 194.84% for the imprint and outer layer catalyst samples respectively versus the square grid sample with 177.38% recovery. Both the imprint and outer layer catalyst samples used 1 gram of catalyst. The outer layer catalyst sample, however, had a larger volume for the catalyst to distribute, resulting in a lower concentration of catalyst located in the area where the cracking would occur. Similar recovery results between the imprint and outer layer catalyst samples signify that when using the imprint method, one could reduce the amount of catalyst used to match the concentration achieved for outer layer catalyst samples and still achieve fully healed samples.

CHAPTER 5: CONCLUSIONS

This thesis documents new methods for the creation of self-healing vascular networks that optimize both the storage and transport processes of the healing agent within wind turbine blades. The goal of the self-healing vascular network is to reduce the costs associated with wind turbine blade damage by instilling the ability to self-heal autonomously. The optimized method involved VARTM Grubbs' first-generation catalyst infused FRP composites embedded with paraffin wax coated copper wiring. The extraction of the copper wiring formed cavities throughout the FRP composite that when injected with the healing agent, DCPD created a self-healing vascular network. The vascular network offers a 100% storage efficiency which is substantially higher than current methods using borosilicate pipettes and microcapsules. The most advantageous of the network configurations, a unilateral network parallel to the VARTM flow, offered an average recovery of 80.92% with a flexural strength of 287.18 MPa, a 3.91% strength reduction in comparison to the control sample. UV reactive dye mixed into the healing agent displayed the vascular networks ability to transport DCPD to both small-scale crack and larger fracture zones. Unlike methods involving microcapsules, the vascular network provides a healing agent reservoir that allows transport to crack sites where following damage events occur and gather healing agent for more extensive fractures. To determine how effective the wire formed network would be when healing an actual wind turbine blade, a test wind turbine was fabricated utilizing the unilateral network and was installed in a wind tunnel producing a 16.5 m/s wind speed. Raman spectroscopy was able to verify that the resulting fracture that occurred within the tunnel was successfully healed by the network. Examing Raman spectra obtained, an estimated 84% of healing agent successfully reacted with the Grubb's first-generation catalyst to create the thermoset PDCPD correlating with the flexural test results' average recovery. The wire

method removes the need for a vessel to house healing agent and thus the decrease in strength caused by the presence of the vessel within the sample. However, the process is still laborious, requiring the careful placement and removal of the wire before to DCPD injection. Moreover, the vascular network created is still formed from individual reservoirs limiting the amount of DCPD available throughout the structure.

The use of 3D printing technology allows freedom when generating the structure of the vascular network. Imprinted vascular networks can precisely control healing agent distribution and concentration. Furthermore, the use of an embedded layer confines the catalyst to a smaller volume. Constraining the catalyst to a small volume maintains the needed concentration for self-healing while reducing the total amount of catalyst needed. The catalyst is focused on where cracks are most likely to propagate rather than the entire FRP sample. Constraining the catalyst to a small volume maintains the needed concentration for self-healing while reducing the total amount of catalyst needed. The catalyst is focused on where cracks are most likely to propagate rather than the entire FRP sample.

Flexural testing shows that samples created using the imprint method had a maximum average recovery percentage of 202.89% for the hexagonal grid with catalyst infused imprint layer sample. In comparison to the wire removal method for creating self-healing networks, the presented method offers a maximum average recovery of 83.32% for penultimate recovery layers. This method remedies the flaws of other methods by creating a single layer interconnected vascular network. Like the wire method, the storage efficiency is 100% meaning no reduction in strength due to the presence of a vessel to house healing agent. Lastly, the imprint method allows for the creation of the imprint layer on the mass scale easily through 3D

printing removing the manual factor for instilling self-healing ability. Using this method, custom vascular networks can be installed in wind turbine blades vascular network structures and tailored to focus DCPD where blades are most prone to failure. Furthermore, this research shows that catalyst need not be dispersed throughout the entire FRP structure to promote self-healing, reducing the cost to instill healing capabilities within blades.

CHAPTER 6: FUTURE WORK

An in-depth study using the imprint method to create optimal vascular network geometries other than the documented hexagonal and square grid configurations. Only two grid geometries were trialed to evaluate the imprint method not to create an ideal configuration to optimize both sample strength and healing recovery.

A method is needed to prevent any premature reaction between the DCPD and the catalyst when the catalyst is dispersed within the imprint layer. Prolonged exposure to catalyst even when DCPD is in its solidified state will start to react with the catalyst to produce PDCPD. With more DCPD available the likelihood of successful crack healing is higher.

An improved process to seal the DPCD once distributed into the imprint layer is needed. The current method relies on perforated plastic sheeting to prevent lamination during flexural testing. Ideally, a coating that would not react with the DCPD but firmly adhere with the surrounding epoxy.

REFERENCES

[1] R. Shen, R. Amano, G. Lewinski and A. K. K. Matt, "New Vascular System Highly Efficient in the Storage and Transport of Healing Agent for Self-Healing Wind Turbine Blades," *Energy Resour. Technol,* vol. 141, no. 5, pp. 051212-051212-8, 2019.

[2] R. Amano, "Review of wind turbine research in the 21st century," *Journal of Energy Resources Technology,* vol. 139, no. 5, 2017.

[3] M. M. Tarfaoui, O. R. Shah and M. M. and Nachtane, "Design and Optimization of Composite Offshore Wind Turbine Blades," *ASME J. Energy Resour. Technol.,* vol. 141, no. 5, p. 051204, 2019.

[4] O. Yuji and W. A. and Koichi, "New Approach Toward Power Output," *ASME J. Energy Resour. Technol.,,* vol. 141, no. 5, p. 051203, 2019.

[5] D. Astolfi, F. Castellani and L. and Terzi, "Definition and Interpretation of," *ASME J. Energy Resour. Technol.,* vol. 141, no. 5, p. 055501, 2019.

[6] T. Simla, W. Stanek and L. and Czarnowska, "Thermo-Ecological Cost of," *ASME J. Energy Resour. Technol.,* vol. 141, no. 3, p. 031201, 2018.

[7] Brøndsted, P., Lilholt, H., &. Lystrup and A., "Composite materials for wind power turbine blades. Annual Review of Materials Science," vol. 35, no. 1, pp. 505-538, 2005.

[8] S. White, N. Sottos, P. Geubelle, J. Moore, M. Kessler, S. Sriram and E. B. a. S.Viswanathan, "Autonomic Healing of Polymer Composites," *Nature,* vol. 409, no. 6822, pp. 794-797, 2001.

[9] Toohey, K. S., Sottos, N. R., Lewis, J. A., Moore, J. S., a. White and S. R., "Self-Healing Materials with Microvascular Networks," *Nature materials,* vol. 6, no. 8, pp. 581-585, 2007.

[10 J. Hansen, C. &. Wu, W. &. S. Toohey, K. &. Sottos, N. &. White, S. &. Lewis and Jennifer, "Self-Healing Materials with Interpenetrating Microvascular Networks," *Advanced Materials,* vol. 21, no. 41, pp. 4143-4147, 2009.

[11 Patrick, J. F., Hart, K. R., Krull, B. P., Diesendruck, C. E., Moore, J. S., White, S. R., a. Sottos and N. R., "Continuous Self-Healing Life Cycle in Vascularized Structural Composites," *Adv. Mater,* vol. 26, no. 25, pp. 4302-4308, 2014.

[12 Motuku, M., Vaidya, U. K., a. Janowski and G. M., "Parametric Studies on Self-Repairing Approaches for Resin Infused Composites Subjected to Low-Velocity Impact," *Smart Mater. Struct.,* vol. 8, no. 5, pp. 623-638, 1999.

[13 A. K. K. Matt, Beyhaghi, S., Amano, R., &. Guo and J., "Self-healing of wind turbine blades using micro-scale vascular vessels," *ournal of Energy Resources Technology,* vol. 139, no. 5, 2017.

[14 A. K. K. Matt, S. Strong, T. ElGammal and R. S. Amano, "Development of Novel Self-Healing Polymer Composites for Use in Wind Turbine Blades," *Energy Resour. Technol,* vol. 137, no. 5, p. 051202, 2015.

[15 A. K. K. Matt, "Advanced Self-Healing Polymer Composites for Wind Turbine Blades," *ProQuest Dissertations and Theses,* vol. 1286, 2016.

[16 Kessler, M. R., Sottos, N. R., a. White and S. R., "Self-Healing Structural Composite Materials;" Composites Part A," vol. 34, no. 8, pp. 743-753, 2003.

[17 ASTM, "Standard Test Method for Flexural Properties of Polymer Matrix Composite Materials," in *Standard No. ASTM D7264/D7264M-15*, West Conshohocken, PA: ASTM International, 2015.

[18 M. R. Kessler, "Characterization and performance of a self -healing composite material," *ProQuest Dissertations and Theses,* 2002.

[19 C. Elanchezhian, V. Ramnath and J. Hemalatha, "Mechanical Behaviour of Glass and Carbon Fibre Reinforced Composites at Varying Strain Rates and Temperatures," *Procedia Materials Science,* vol. 6, no. 2014, pp. 1405-1418, 2014.

[20 Zedler, L., Hager, M. D., Schubert, U. S., Harrington, M. J., Schmitt, M., Popp, J. and B. Dietzek, "Monitoring the chemistry of self-healing by vibrational spectroscopy – current state and perspectives," *Materials Today,* vol. 17, no. 2, pp. 57-69, 2014.

[21 Schaubroeck, D., Brughmans, S., Vercaemst, C., Schaubroeck, J., &. Verpoort and F., "Qualitative FT-Raman investigation of the ring opening metathesis polymerization of dicyclopentadiene," *Journal of Molecular Catalysis A Chemical,* vol. 254, no. 1–2, pp. 180-185, 2006.

[22 Ding, S. X., Yan, C. Y., Min, Z. R., &. Ming and Q. Z., "Self-healing epoxy based on cationic chain polymerization," *Polymer,* vol. 50, no. 13, pp. 2967-2975, 2009.

[23 MatWeb, "Overview of materials for Polydicyclopentadiene (PDCPD)," MatWeb, [Online]. Available: http://www.matweb.com/search/datasheet.aspx?matguid=16d3d6b1e32c4c368fa1ddac6afb2b93&ckck=1. [Accessed 22 May 2019].